Oxidation catalysis by iron and manganese porphyrins within enzyme-like cages

Journal:	*Biopolymers*
Manuscript ID	Draft
Wiley - Manuscript type:	Review
Date Submitted by the Author:	n/a
Complete List of Authors:	Chino, Marco; Universita degli Studi di Napoli Federico II, Chemical Sciences Leone, Linda; Universita degli Studi di Napoli Federico II, Chemical Sciences Zambrano, Gerardo; Universita degli Studi di Napoli Federico II, Chemical Sciences Pirro, Fabio; Universita degli Studi di Napoli Federico II, Chemical Sciences D'Alonzo, Daniele; Universita degli Studi di Napoli Federico II, Chemical Sciences Firpo, Vincenzo; Universita degli Studi di Napoli Federico II, Chemical Sciences Aref, Diaa; Universita degli Studi di Napoli Federico II, Chemical Sciences Lista, Liliana; Universita degli Studi di Napoli Federico II, Chemical Sciences Maglio, Ornella; Universita degli Studi di Napoli Federico II, Chemical Sciences; National Council of Researches, IBB Nastri, Flavia; Universita degli Studi di Napoli Federico II, Chemical Sciences Lombardi, Angela; Universita degli Studi di Napoli Federico II, Chemical Sciences
Keywords:	heme-protein models, Oxidation catalysis, Bioinorganic chemistry, Protein design, Metal-metalloporphyrin framework

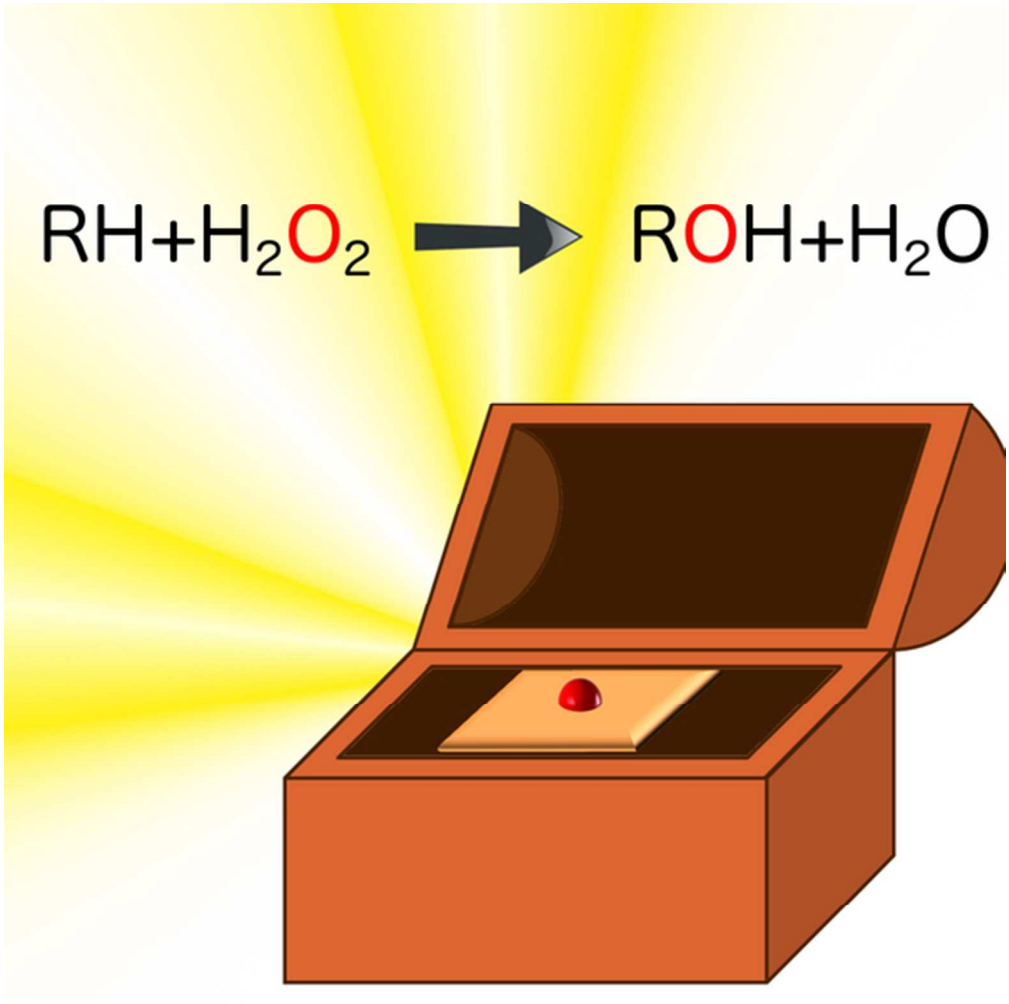

50x50mm (300 x 300 DPI)

Oxidation catalysis by iron and manganese porphyrins within enzyme-like cages

Marco Chino,[1] Linda Leone,[1] Gerardo Zambrano,[1] Fabio Pirro,[1] Daniele D'Alonzo,[1] Vincenzo Firpo,[1] Diaa Aref,[1] Liliana Lista,[1] Ornella Maglio,[1,2,*] Flavia Nastri[1,*] and Angela Lombardi[1,*]

[1] *Department of Chemical Sciences, University of Napoli "Federico II", Via Cintia, 80126 Napoli (Italy)*

[2] *IBB - National Research Council, Via Mezzocannone 16, 80134 Napoli (Italy)*

Correspondence to: Angela Lombardi; e-mail: alombard@unina.it
Flavia Nastri; e-mail: flavia.nastri@unina.it
Ornella Maglio; e-mail: ornella.maglio@unina.it

Abstract

Inspired by natural heme-proteins, scientists have attempted for decades to design efficient and selective metalloporphyrin-based oxidation catalysts. Starting from the pioneering work on small molecule mimics in the late 1970s, we have assisted to a tremendous progress in designing cages of different nature and complexity, able to accommodate metalloporphyrins. With the intent of tuning and controlling their reactivity, more and more sophisticated and diverse environments are continuously exploited. In this review, we will survey the current state of art in oxidation catalysis using iron- and manganese-porphyrins housed within designed or engineered protein cages. We will also examine the innovative metal-organic framework (MOF) systems, exploited to achieving an enzyme-like environment around the metalloporphyrin cofactor.

Key words: Heme-protein models; Metal-metalloporphyrin framework; Oxidation catalysis; Bioinorganic chemistry; Protein design

Contents

1. Introduction

In 2001, some of us shared with Vincenzo Pavone the drafting of the review "Peptide-based heme-protein models", featured on *Chemical Reviews*.[1] In this review, several key concepts on spectroscopic and coordination properties of metalloporphyrins, together with protein design strategies aimed at developing heme-protein models, were described. The literature reviewed in that paper clearly showed the feasibility of constructing peptide-based heme-protein mimetics through different approaches. Indeed, in almost two decades, heme-protein design has exponentially grown, thus testifying how still vital and vibrant remains the research field on one of the "oldest" topics in bioinorganic chemistry.[2–9]

Natural heme-containing enzymes perform catalysis in water, under mild conditions, and in most cases with second order rate constants that are limited only by the diffusion of the substrates (catalytic efficiency k_{cat}/K_M ranging from 10^4 to 10^9 $M^{-1}s^{-1}$).[10] Moreover, their high chemio-, regio- and stereo-selectivities accounts for the involvement of heme-enzymes in the most important biological processes supporting life. Cytochromes P450 perform monooxygenation reactions adopting O_2 as the oxygen source.[11] Heme oxygenase activates O_2 at a heme center to catalyze its own degradation.[12] Peroxidases, such as cytochrome *c* peroxidase (CcP) or horseradish peroxidase (HRP), and catalases, such as bovine serum catalase, reduce hydrogen peroxide to water by oxidizing cytochrome *c*, phenolic compounds and hydrogen peroxide itself, respectively.[13] Cytochrome *c* oxidase (C*c*O) is the terminal enzyme of the respiratory chain in mammals,[14] catalyzing the net four-electron reduction of dioxygen to water, which is coupled to the proton flux necessary for ATP synthesis. Nitric oxide reductase (NOR)

reduce NO for energy production in some bacterial strains,[15] whereas nitric oxide synthase (NOS) produce NO from the oxidation of arginine for cellular signaling and immune defense in mammals.[16]

It is therefore evident that Nature mastered coordination chemistry in such a way that a single cofactor (and slight modifications thereof) could access to a wide range of reactivities.[17] Bioinorganic chemists tackled the challenge to unravel the mechanisms that allow the protein matrix to modulate the catalytic activity of metal-containing cofactors, through the development of artificial systems.[4,9,18–30] Their performances replicate and, in some exciting cases, overcome the kinetic parameters of the natural counterparts.[31–35]

In the case of heme-proteins, the cofactor alone is able to recapitulate the enzymatic reactivity, though in organic solvents and under harsh conditions.[19,36] Several outstanding results have been obtained by chemical modification of the porphyrin ligand in the tuning of the electronic structure, the solubility in aqueous solvent, the substrate recognition, and the regio- and stereo- specificity.[19,36–38] A very recent review by Goldberg and coworkers illustrates the biomimetic reactivity of iron- and manganese-porphyrinoid systems, and the improvements in the field.[36] Nevertheless, it is still difficult to design a small catalyst with high catalytic efficiencies for practical applications, since different level of complexity around the macrocycle should be needed.

The last two decades have seen progress in designing elaborate scaffolds, able to accommodate metallo-porphyrins, and to tune their functions. The scope of this review is to outline the performance in oxidation catalysis, reached by iron- and manganese-porphyrins when housed within designed or engineered enzyme-like cages. After a brief discussion on the main features of iron and manganese when inserted into porphyrins

(Section 2), and their relation to the reaction pathways of heme-enzymes active in oxidation catalysis (Section 3), we will review the approaches used to develop model systems (Section 4). We categorize these models by considering the covalent or non-covalent anchoring of the porphyrin within the peptide/protein scaffolds (Figure 1A-B). Description will focus on systems developed either by protein design and redesign, cofactor replacement, or cofactor insertion.

Even though peptides and proteins are Nature's favorite building blocks for modulating metalloporphyrin reactivity, there is still room for further innovation. Several macromolecules and/or supramolecular systems have been used so far for the development of metalloporphyrin conjugates with different properties.[39–42] Among them, we will report, in section 5, the innovative strategies based on the construction of metalloporphyrin-based metal-organic frameworks (MOF).[43] From MOF examples we will see that, by a supramolecular approach, functional environments around cofactors could recapitulate the features of a protein core (Figure 1C).

2. Iron and manganese: the "Lords of the rings"

Water exchange rate at several aqueous metal complexes of the first transition series is very fast, making metal complexation in water a very difficult task.[44] Moreover, the solubility of metal hydroxides is very low.[45] Nature adopted porphyrins as ligands to trap the chemical potential of metal ions in water. The extended aromatic framework makes porphyrins relatively stable and inert, even under harsh conditions of temperature and oxidative stress.[46] Further, stability of their metal complexes is a consequence of the macrocycle chelate effect, as well as of back-bonding interaction.

Porphyrin metal-complexes are known for any metal of the first transition series, in several oxidation states, and with different geometries, depending on the ionic radius.[46] Nevertheless, iron and manganese represent the most suitable choices both in terms of oxygen activation and environmental sustainability. Being in the middle of the *d*-block, both metal ions have access to a wider range of oxidation states. These states can be readily tuned, as well their chemistries both in terms of Lewis acidity and hardness/softness.[17,45] Nature is "leader" in doing this, making iron able to reduce dioxygen and manganese able to oxidize water.[14,47]

At neutral pH, iron and manganese in porphyrin complexes are stable as formal trivalent cations (M^{3+}Por; M=Fe or Mn). This is somehow unexpected when considering that aqueous iron(III) has a much lower of aqueous manganese(III) ($E_0(Fe^{3+}/Fe^{2+})$ = 0.77V; $E_0(Mn^{3+}/Mn^{2+})$ = 1.54V).[48] This behaviour clearly demonstrate the effects of the ligand field exerted by the porphyrin on the electronical structure of the metals, which in turn differently modulate their reduction potentials.

In porphyrin-based model compounds, the reduction potentials may vary between -200 and +500 mV (vs SHE), depending on the presence of electron-withdrawing groups as substituents of the porphyrin ring, which favor lower oxidation states.[49,50] The limited number of natural heme cofactors narrows the range of accessible potentials for heme-proteins. Therefore, the protein scaffold modulates the redox potential by selecting the axial ligands and/or the residues surrounding the heme.[17] Most importantly, thanks to the dynamic nature of the protein chain, every modulating mechanism can be triggered upon "request".[51,52] In some cases, the scaffold allows also distortions of the porphyrin ring or stabilizes exogenous substrates that are able to change the chemical environment around

the cofactor. The effects of both porphyrin frameworks and protein scaffold in tuning the metal-cofactor redox potential are well exemplified by the comparison between native and Mn-reconstituted myoglobin.[53,54] The redox potential of the iron center in myoglobin (60 mV vs SHE) stabilizes the Fe(II) by ~200 mV (with respect to the free hemin), highlighting the need for Mb to cycle between the two redox state to exert its dioxygen binding function.[53]

Manganese reconstituted myoglobin has a much lower redox potential (-121 mV vs SHE), explaining the nature choice of iron for dioxygen binding. Moreover, the effect exerted by the protein matrix stabilizes the lower oxidation state to the same extent as with iron.[54] This simple example highlights that, independently by the cofactor, protein contribution to the reduction potential could be considered as additive and, in principle, predictable.

The next section will illustrate how natural enzymes tweak the electronic structure of iron to selectively perform oxygen activation.

3. Heme-enzymes and oxidation catalysis

In coordination chemistry, one possible way to manage the metal propensity to perform one- or two-electron transfer processes is to adopt "non-innocent" ligands, which may delocalize the spin density and/or may provide proton shuttling.[55] In this perspective, oxygen-activating heme-enzymes can be viewed as the paradigm of the mechanisms adopted by Nature to tune the metal cofactor, to selectively perform one process over the other. A comprehensive description of the structure-function relationships of these heme-enzymes is beyond the scope of this review, and readers can refer to recent excellent

reviews on this argument.[51,56] Herein, by looking at oxygen-activating heme-enzymes, we will try to dissect the minimal requirements that a heme-protein model should embody to function in catalysis.

There is general agreement about the heme paradigm of oxidation (Figure 2), though few exceptions in the definition of the intermediates may arise for some enzymes.[38,51] Four main classes of reaction (highlighted with different colors in Figure 2) can be identified, each one reaching a specific step of this special stairway:

(1) superoxide dismutation (pink arrows);

$$2O_2^{\cdot-} + 2H^+ \rightleftarrows O_2 + H_2O_2$$

(2) catalase/hydrogen peroxide dismutation (green arrow);

$$2H_2O_2 \rightleftarrows O_2 + 2H_2O$$

(3) oxidase/peroxidase (blue arrows; D denotes an electron donor substrate);

$$2D + O_2 + 4H^+ + 2e^- \rightleftarrows 2D^{\cdot+} + 2H_2O$$

$$2D + H_2O_2 + 2H^+ \rightleftarrows 2D^{\cdot+} + 2H_2O$$

(4) oxygenase/peroxygenase (red arrows).

$$RH + O_2 + 2H^+ + 2e^- \rightleftarrows ROH + H_2O$$

$$RH + H_2O_2 \rightleftarrows ROH + H_2O$$

In superoxide dismutation, superoxide anion binds the resting state to form a superoxo intermediate, which is in equilibrium with the oxy-form, thus releasing dioxygen and the reduced cofactor (Figure 2, pink arrow on the right). This species may then reduce a second equivalent of superoxide to release hydrogen peroxide, both through an outer or an inner sphere electron transfer process (Figure 2, pink arrow on the left). In order to take place, the catalyst must interact with the negatively charged superoxide anion. For

this reason, positively charged catalysts are more prone to interact with this substrate. However, the resulting electron-withdrawing environment may cause with a reduction potential of the metal center too high for the second step (superoxide reduction) to take place.[50] Finally, the released hydrogen peroxide should not interfere by sequestering the oxidized form of the catalyst. A good superoxide dismutation catalyst should therefore have: (i) a redox potential for the M(III)/M(II) couple lying between the potentials of oxidation and reduction of the superoxide; (ii) a positive substrate binding site; (iii) low-affinity for hydrogen peroxide. In this respect, manganese is much more indicated than iron, its lower redox potential allows addition of a positively charged binding site, and Mn(III) is less prone to react with hydrogen peroxide at neutral pH.[57]

A peroxo intermediate is shared among the catalytic cycles in the three subsequent reactions catalyzed by heme. The peroxo intermediate may be generated both by direct coordination of hydrogen peroxide (peroxide shunt, black dashed arrow in Figure 2), or by a preactivation step consisting in a two-electron reduction of dioxygen, as in cytochrome P450 and NOS. This intermediate may then evolve by heterolytic scission of the O-O bond. This produces a water molecule and a formal $[M(IV)=O(Por)]^{\bullet+}$ intermediate, also called compound I. At this stage, a subtle interplay of electron configuration, proton shuttling, and substrate affinity determines the preferred catalytic route. When the metal is manganese(III), its high-spin porphyrin complexes exert a weaker electron-withdrawing effect on the axial ligand, due to their lower reduction potential. For this reason, its interaction with hydrogen peroxide is expected to be weaker than iron-porphyrins, as previously anticipated. Manganese is therefore less efficient than iron in lowering the pKa of hydrogen peroxide, which is needed for its heterolytic

cleavage and compound I formation. Two possible ways to overcome this limitation would be by increasing the pH or by directly reducing its superoxo intermediate.

Catalases catalyze hydrogen peroxide dismutation. The first hydrogen peroxide equivalent is converted to water and compound I, the latter then oxidize a second equivalent to dioxygen (Figure 2, green arrow), a two-electron transfer process. Peroxidases, such as horseradish peroxidases (HRP), instead, catalyze oxidation of organic substrates by two separate one-electron reductions of compound I (Figure 2, blue arrows). Promiscuity between these two reactivities is very difficult to overcome, and even natural peroxidases still present residual catalase activity.[58,59] In some cases, catalase cycle has been invoked for peroxidases as a protective mechanism against auto-inactivation.[58] Intensive characterization of these proteins has identified some key features: (i) in catalase the metal cofactor is deeply embedded in the protein scaffold, thus protecting from outer-sphere electron transfer processes; (ii) a narrow channel allows only small diatomic molecules to enter the active site; (iii) a deprotonation mechanism supports dioxygen release; (iv) in catalase the ligand field effect of the tyrosinate axial ligand is stronger than histidine in peroxidases, exerting a "push" effect on the compound I, which decreases its electron affinity but increases its ability to abstract hydrogen.

Oxygenation and peroxygenation activities consist in the oxidation of a substrate by insertion of an oxygen atom coming from dioxygen or hydrogen peroxide, respectively (Figure 2, red arrows). Cytochrome P450 and chloroperoxidase are very well studied representatives of these two classes of enzyme. In P450s, the substrate binding triggers the reaction cycle, by shifting the spin of the resting state from low-spin to high-spin. This shift lowers the redox potential, thus allowing the first reduction to occur. The high-

spin iron(II) interacts with dioxygen, generating the superoxo intermediate. The superoxo is then reduced to the peroxo intermediate, whose fate has been already discussed. In order to accomplish these tasks, Nature has selected a cysteinate as fifth ligand. The sulphur atom is a soft ligand and stabilizes the softer high-spin iron(II). Further studies have highlighted the role of cysteine that acts as an electron pump for the metal.[51] In such perspective, sulphur provides lower energetic barriers to oxidation/reduction if compared to second period elements, such as nitrogen and oxygen. Once reached the compound I intermediate, oxygenating enzymes are able to abstract a hydrogen atom from the strong aliphatic C-H bond, with the concomitant formation of a short-lived substrate radical and the compound II species. Though formally similar, the P450 compound I shows some crucial electronic differences with respect to the peroxidase one: (i) the cysteinate fifth ligand exerts a strong push to the metal-oxo moiety, lowering its electron affinity; (ii) electron-donating cysteinate increases the pKa of compound II by increasing the Fe-O distance, favoring the H atom abstraction; (iii) the apolar distal site increases the compound II pKa, which is protonated in oxygenases. The differences of compound I/compound II couple are related to their reduction potential. The two-electron reduction potentials ($E'_{cpd\ I/ferric}$) are similar between peroxidases and (per)oxygenases (0.95 V for HRP; 1.1 V for chloroperoxidase). This enables both to oxygenate thioanisole, or epoxidate alkenes, processes lacking the hydrogen abstraction step.[60,61] The two one-electron potentials were estimated to be equivalent in peroxidases, whereas an imbalance was observed in (per)oxygenases. The protonation of the ferric-oxo intermediate accounts for the higher first ($E'_{cpd\ I/cpd\ II}$) potential. Such higher potential would then give the driving force for the C-H bond activation of aliphatic substrates.

The lessons learned so far from the study of natural proteins are very useful for the design of new tailor-made catalysts. However, there are still some unclear aspects, and the bottom-up approach of model design, here reviewed, has demonstrated its proficiency in deepening our understanding of oxygen activation.

4. Heme-Protein model based on covalent peptide-porphyrin systems

Covalent protein/peptide-porphyrin systems offer the advantage of tightly positioning the cofactor inside the protein environment. The covalent linkage prevents metal-cofactor dissociation phenomena and reduces the possibility of axial ligand dissociation and/or scrambling. Numerous strategies have been developed to afford elaborated peptide-porphyrin architectures.[62,63] The systems herein described point out that an increase in the catalytic activity is strictly related to the complexity of the cofactor environment.

SOD activity has been widely reported in very simple Mn-porphyrins.[50,64] Their covalent conjugation to peptides or proteins can afford molecules able to protect cells from oxidative stress. Asayama and coworkers developed a cationic Mn-porphyrin–catalase conjugate with the dual function of SOD and catalase (Figure 3).[65] Conjugation of the two moieties slightly altered their individual reactivities (Mn-porphyrin alone $k_{SOD} = 8.0 \times 10^6$ M^{-1} s^{-1}, Catalase alone $k_{CAT} = 4.0 \times 10^7$ M^{-1} s^{-1}; conjugate $k_{SOD} = 1.7 \times 10^7$ M^{-1} s^{-1}; $k_{CAT} = 2.3 \times 10^7$ M^{-1} s^{-1}), and afforded a system that efficiently work for multi-electron reduction of $O_2^{\bullet-}$ to H_2O. In a subsequent paper, the same Mn-porphyrin was conjugated to a mitochondrial signal peptide for cell targeting.[66] Also in this case, conjugation was

proficient in affording a good SOD catalyst, which could protect mitochondria from oxidative damage.

These examples prove the minimal requirements for SOD activity, as previously outlined in section 3. The conjugation with peptides/proteins was only aimed at enhancing the delivery of the complex toward cellular targets.

Conversely, to reproduce peroxidase activity in model systems, it is necessary to construct more complex architectures, mimicking both the first and second shell interactions. Such interactions account for the cofactor ability to process H_2O_2 in selective substrate oxidation.

The work by Umezawa and coworkers support this concept. Using versatile copper-catalyzed azide-alkyne cycloaddition, they prepared nine peptide-Mn-porphyrin conjugates as artificial catalases.[67] They elegantly synthesized a porphyrin with four 5-azido-3-pyridyl- groups at the *meso* positions, which were conjugated to a selection of propiolic acid N-capped peptides. Peptides corresponded to scrambled sequences of Gly, Lys, Glu, His and Citrulline (Cit). The resulting conjugates were assayed for both catalase and peroxidase activity. Only a very small enhancement of the catalase activity, respect to a control positive Mn-porphyrin, was observed for the derivative containing the positively charged -Lys-Gly-Cit-NH_2 sequence. Interestingly, the only derivatives active as peroxidases contained the negatively charged Glu residue, or His. This small system exemplifies the effect of charged residues on pathway selectivity. For instance, the Cyt ureido group can drive toward catalase activity by stabilizing H_2O_2 through hydrogen bonding, as already observed in Mn salen complexes.[68]

Microperoxidases (MPs) are a class of covalent peptide-porphyrin systems, obtained upon cytochromes c proteolytic cleavage.[69] They consists of a short peptide chain, generally from 6 to 11 residues, covalently bound to heme c through two Cys residues of a Cys-Xxx-Xxx-Cys-His motif. Despite their small size, MPs bear first coordination sphere interactions through the His residue, acting as axial ligand to the heme iron, (Figure 4). Thus, they embody minimal structural requirements for function as heme-protein mimics. Indeed, several MPs were proved to catalyze oxidation and oxygenation reactions, such as aromatic hydroxylation, oxidative dehalogenation, tioether sulfoxidation and the oxidative coupling of phenolic substrates.[70–73]

A limitation to the use of MPs as homogeneous catalysts is the presence of a degradative pathway, causing porphyrin bleaching during catalysis. However, they have being useful to well elucidate the effect of the intrinsic nature of the metal ion in modulating heme-protein activity.[74–76] Mn(III)-MP-8 is less efficient than Fe(III)-MP8 in H_2O_2 deprotonation, as revealed by the pH dependence of the kinetic constant for compound I intermediate formation (pK_a 9.2 and 11.0 for iron and manganese, respectively).[75] Thus, Mn(III)-MP-8 peroxidase activity is observed at pH values 2-3 units higher than Fe(III)-MP8. Another important outcome from MP8 is the effect of iron to manganese substitution in directing the catalyst toward peroxidase-like or P450-like reactions, upon H_2O_2 activation. Manganese insertion shifts the reduction potential to 154 mV lower than iron ($E_0(Fe^{3+}/Fe^{2+})$ = 361 mV; $E_0(Mn^{3+}/Mn^{2+})$ = 207 mV). This in turns increases the kinetic stability of the Mn-oxo compounds I and II and reduce their reactivity for electrophilic attack on substrates. The global effect is that Mn(III)-MP8 has a lower reactivity in oxygen transfer reactions.

In addition to the axial ligand, engineering of the distal side is an important requirement for achieving a successful catalyst approaching the efficiency of natural systems.[17] Through a miniaturization process, our research group developed a class of heme-protein models named Mimochromes.[1] The prototype molecule (Mimochrome I) contains two identical nonapeptides covalently linked to deuteroporphyrin through amide bonds between the heme-propionic groups and the ε-amino groups of lysine residues. Peptide sequence was patterned on the F helix of hemoglobin β-chain. Each peptide bears a histidine axial ligand to the heme iron, leading to a *bis*-His coordination, with a helix-heme-helix sandwiched structure. Starting from Mimochrome I, a careful redesign process was carried out, and numerous analogues were developed to improve structural and functional properties. Among them, Mimochrome IV displayed an increased solubility respect to Mimochrome I (in the range of 10^{-3} M in aqueous solution) and a very stable structure; it also represents the first miniaturized protein for which both solution NMR and X-ray crystal structure of the cobalt(III)-complex have been solved.[77,78] Based on the results on symmetrical hexa-coordinated complexes, subsequent design was focused on creating asymmetrical penta-coordinated analogues apt to perform oxidative catalysis. Fe(III)-Mimochrome VI was the first model of the series to show peroxidase-like activity.[79,80] Unlike its precursors, Mimochrome VI mimics the asymmetry of natural proteins in both primary and secondary coordination spheres. It is made up of a tetradecapeptide (*TD*) bearing the His axial ligand, and a decapeptide (*D*) lacking metal-coordinating residue, which allows to create a substrate binding pocket on the distal side of the heme. Fe(III)-Mimochrome VI behaves like a very efficient artificial peroxidase, since it catalyzes the oxidation of (ABTS) and guaiacol with catalytic

efficiencies (k_{cat}/K_m= 4.42 $\times 10^6$ (ABTS); 8.70 $\times 10^5$ (guaiacol) M^{-1}/s^{-1}) comparable to those of natural horseradish peroxidase (HRP) in the conditions of maximal activity for each catalyst. Fe(III)-Mimochrome VI also converts phenol to 2- and 4-nitrophenol in presence of H_2O_2 and NO_2^-, with high reaction yields.

The results obtained with Fe(III)-Mimochrome VI demonstrate the key role of the *D* chain in protecting the catalyst from bleaching. Next, we tried to introduce more functional features into the Mimochrome scaffold, by focusing on two second-shell interactions which were demonstrated to be crucial in the formation and stabilization of the high-valent oxo-ferryl species (Compound I) during catalysis: 1) the hydrogen bond between the proximal His axial ligand and an Asp side-chain, which is known to exert the so called "push effect"; 2) the distal side Arg residue, which is proven to assist the cleavage of the O–O peroxide bond.[51] Punctual mutation of specific amino-acid residues into Fe(III)-Mimochrome VI structure were performed (Figure 5A). Particular attention was devoted to the N- and C-terminal charged residues (Glu^2 and Arg^{10}, respectively) in both peptide chains, which were intended to stabilize secondary and tertiary structures through inter-chain electrostatic interactions. Substitution of Glu^2 with a hydrophobic Leu on the proximal tetradecapeptide was introduced, thus leaving unpaired the positively charged Arg^{10} on the distal side of the heme. This mutation led to a 4-fold enhancement of the catalytic efficiency (k_{cat}/K_m= 1.60 $\times 10^7$ $M^{-1}s^{-1}$) in the ABTS oxidation, overcoming that of HRP.[80] Thus, the analog E^2L(*TD*)-Fe(III)-Mimochrome VI behaves like natural peroxidases, whose reactivity is similarly influenced by the proximal and distal heme environments. Moreover, it shows a peroxidase-like mechanism, through the formation of compound I, containing a Fe(IV)=O center and a porphyrin radical

cation. This molecule is currently under redesign process to screen the effect of other mutations, as well as of manganese insertion, on catalytic performance.

Following a very similar approach to Mimochrome design, Venanzi and coworkers recently reported a biomimetic oxidation catalyst (FemP(10N)$_2$) by conjugation of a Fe(III)-mesoporphyrin with two α-helical decapeptides.[81] Amphiphilic peptide sequences, made up of Aib and Glu residues, were designed to ensure porphyrin water-solubility and create a cavity near the porphyrin core for substrate recognition and catalysis. They were interested in evaluating the catalytic performances of a model lacking His as fifth ligand. Spectroscopic studies and molecular mechanics calculations indicated that the heme could be axially coordinated by one or two Glu side-chains. FemP(10N)$_2$ was able to promote the oxidation of both D- and L-Dopa to dopaquinone, performing several turnovers without bleaching. A higher value of the K_M for the L-Dopa was observed, suggesting a weak stereoselectivity of the catalyst. This effect was mainly attributed to the conformationally constrained structure of the two peptides. However, the lack of tuning exerted by the axial ligands could account for the observed small catalytic efficiencies in H_2O_2 activation (k_{cat}/K_M = 3-5 $\times 10^5$ $M^{-1}s^{-1}$).

Increasing the complexity of the peptide moieties around the porphyrin allows for more interactions to be inserted and screened for activity. In this respect, the use of four-helix bundles as protein cages for mono-heme and multi-heme model systems has been widely reported.[82] Our group exploited the use of this structural motif in the design of MiniPeroxidase 3 (MP3), a catalyst with peroxidase activity.[83] Design of MP3 was patterned on the heme-binding motif of bacterioferritin (BFR)[84] (Figure 5B). The original sequence of BFR was modified to engineer an asymmetric α_2-heme-α_2 covalent

sandwich containing: (i) a His residue on one chain that acts as an axial ligand to the iron ion; (ii) a vacant distal site able to accommodate exogenous ligands or substrates; and (iii) an Arg residue in the distal site that should assist hydrogen peroxide activation as in HRP. Fe(III)-MP3 shows high catalytic turnover (k_{cat} =535 s^{-1}) and efficiency (k_{cat}/K_M = 1.57 $\times 10^6$ $M^{-1}s^{-1}$) in the oxidation of ABTS by H_2O_2. However, the observed activity is lower respect to natural HRP, probably due to the mobility of the catalytic Arg in the distal site.

Outstanding results in the use of four-helix bundle to cage heme for tuning peroxidase-like activity were recently reported by Ross Anderson and coworkers.[34] They described the construction of a *de novo* artificial heme-binding *maquette* able to efficiently catalyze oxidation reactions using H_2O_2. *Maquettes* are simple four helix bundles, designed from scratch by Dutton and coworkers, which were able to functions as electron-transfer[85] or oxygen carrier[86] proteins, upon insertion of heme and/or other types of redox-active cofactors.

The Anderson's group demonstrated that artificial *maquettes* can be recognized and modified by the post-translational cytochrome *c* maturation system of *E. Coli* for covalent incorporation of the heme cofactor *in vivo*, affording the "c-type cytochrome *maquettes*" (CTMs).[87] Starting from an existing non-catalytic CTM, a mono-histidine peroxidase-like heme active site was introduced through a simple and few-steps design process (Figure 6).[34] The resulting enzyme, named C45, displays one of the highest catalytic efficiencies toward ABTS oxidation within the artificial peroxidases models developed so far (k_{cat} = 1200 s^{-1}; $K_M(H_2O_2)$ = 94 mM; K_M (ABTS) = 379 μM k_{cat}/K_M= 3.20 $\times 10^6$ $M^{-1}s^{-1}$), and retains its activity also at high temperatures. The lack of a

rationally designed substrate recognition site gives to C45 the ability of promoting a wide array of substrate trasformations as in non-specific natural peroxidases, such as oxidation of guaiacol, luminol, *o*-phenylenediamine, *p*-anisidine, 5-aminosalycilic acid and the oxidative dehalogenation of 2,4,6-trichlorophenol and its brominated and fluorinated analogs. The level of complexity in the protein scaffold will undoubtedly lead to new metalloenzymes tailored for more challenging applications.

5. Non-Covalent heme-protein models using native protein scaffolds

The design of non-covalent heme-protein models has been successfully approached through the use of native protein scaffolds, properly selected to interact with the cofactor. To modulate activity and selectivity, the scaffold should have a suitable cavity for hosting heme, and a stable structure apt to tolerate specific mutations in the heme microenvironment. The following sections describe examples of catalysts developed by heme-protein cofactor replacement and supramolecular anchoring.

5a. Reconstitution of heme-proteins with different porphyrin-like cofactors

Parallel to classical biochemical engineering techniques, as in site-selected mutagenesis, heme substitution became an attractive alternative approach to get deep insights into structure-function relationships of heme-proteins.[3,88] Some slight variation in the porphyrin ring structure have dramatic effects in modulating heme-protein properties.[89] Native heme can be removed from its binding site, and the resulting apo-proteins can be

easily refolded in the presence of a modified heme cofactor, without losing the native folded structure and stability.[7]

The heme cofactor can be modified either at the porphyrin framework, by using porphyrinoid-like cofactors, or at the metal center by metal substitution in the native PPIX, or both. Among native scaffolds, Mb, with its very weak peroxidase and mono-oxygenase activities, is widely used as a white canvas for "painting" new activities.

Hayashi and coworkers were successful in endowing Mb with new functions, by using iron porphycene (Pc) (Fe(III)-Pc, Figure 7), a nonnatural porphyrinoid ligand in which two bipyrroles are linked by two ethylene bridges.[90,91] Reconstituted Mb (rMb) X-ray structure showed that Fe(III)-Pc was bound in the native heme pocket, between E and F helices, with F helix His93 acting as axial ligand. Fe(III)-Pc renders Mb a competent catalyst in the H_2O_2-mediated oxidation of substrates such as guaiacol, thioanisole, and styrene. Indeed, the initial rate of the guaiacol oxidation was 11-fold enhanced respect to WT-Mb at pH 7. Based on spectroscopic and kinetic studies, the authors suggested that a stronger coordination of Fe-His93, (the p$K_{1/2}$, pH value corresponding to 50% dissociation of the prosthetic group, is 3.1 for rMb respect to 4.5 for WT-Mb) and a lower Fe^{3+}/Fe^{2+} redox potential (-190 and +52 mV vs NHE, for rMb and WT-Mb, respectively) account for the observed rMb catalytic activity. Moreover, stopped-flow kinetic analysis in the presence of molar excess of H_2O_2 revealed the formation of two reaction intermediates, i.e. compound II ([Pc-Fe(IV)=O]) and compound III ([Pc-Fe(III)-$O_2^{\cdot-}$])-like species.[91]

Insertion of Fe(III)-Pc into *apo*-HRP was also explored.[92] The reconstituted enzyme (rHRP) exhibited the same catalytic properties of native HRP (nHRP) in the oxidation of

guaiacol, whereas a 12-fold increase of TON was detected for thioanisole H_2O_2-mediated oxidation. The authors suggested that the reason for the poor reactivity toward H_2O_2 was the low-spin character of the ferric Pc. This slower step would then be counterbalanced by the strongly activated ferryl species, as suggested by the measured higher redox potential of the ferryl porphycene.[92]

The same authors investigated the effect of insertion of iron corrole (Figure 7) on the peroxidase activity of both HRP and Mb.[93] The reconstituted proteins (rHRP and rMB) displayed remarkable differences in both electronic configurations and peroxidase activities. The imidazolate nature of the His ligand in HRP[51] likely accounts for the stabilization of a Fe(IV) corrole state in the rHRP, electronically equivalent to a Fe(III) corrole π-cation radical observed in the rMb. This effect could account for the observed reactivity order toward guaiacol oxidation: nHRP > rHRP > rMb > nMb. A Fe(IV) corrole state would disfavor H_2O_2 binding and activation in rHRP, while an extension of the lifetimes of oxidized intermediates could account for the observed rMb peroxidase activity.

Reconstitution approaches have been also focused on providing Mb with an artificial substrate-binding domain.[94] While the introduction of aryl substituents in the propionate groups of protoheme IX already demonstrated to enhance the peroxidase-like activity of the corresponding reconstituted Mb,[94] additional mutation of distal His64 to Asp (H64D) resulted in a 430-fold enhancement of the catalytic efficiency (k_{cat}/K_M) of the reconstituted Mb toward guaiacol oxidation with respect to WT-Mb.[95] More recently, the reconstitution of MbH64D with synthetic hemes substituted at only one of the two propionates ("single winged" cofactor, Figure 8), resulted in an artificial enzyme with a

20-fold increase in the k_{cat} value with respect to MbH64D and with a catalytic efficiency comparable to that of native HRP (rMbH64D: $k_{cat}/K_M = 8.5 \times 10^4$ M^{-1} s^{-1}; HRP: $k_{cat}/K_M = 7.2 \times 10^4$ M^{-1} s^{-1}).[95]

Impressive results were obtained by modifying both the macrocycle and the metal ion. Mb reconstituted with Mn porphycene (Mn(III)-Pc) (Figure 9A) was able to catalyze the H_2O_2-dependent alkane hydroxylation, by converting ethylbenzene in 1-phenylethanol as a single product (Figure 9B).[96] Under the same conditions, WT myoglobin and other modified myoglobins did not show any catalytic activity. Crystal structure showed that Mn(III)-Pc is within the Mb heme-binding pocket, but His93 coordination is weaker respect to WT-Mb (Figure 9A). Kinetic isotopic effect (KIE) experiments suggested that a hydrogen-atom abstraction by a Mn-oxo species is involved in the rate-determining step. A subsequent rebound hydroxylation process would then close the catalytic cycle, very close to cytochrome P450 reaction mechanism.

Simple metal ion substitution in the native porphyrin framework can cause dramatic effect on reactivity, as outlined by Fe to Mn substitution in MP8 (see section 4). Inspired by Watanabe's work on the mutation-dependent reactivity of hemoproteins,[3] Zhang and coworkers developed a variety of Mb distal site mutants to counterbalance the effect of the poor peroxidase reactivity of Mn-PPIX-reconstituted Mb (Figure 10A).[97–99] In particular, mutation of L29, F43 and H64 distal residues were exploited for their effects in promoting ABTS oxidation. Distal H64 was found to play a key role in H_2O_2 binding by H-bonding formation, which facilitates the H_2O_2 coordination to the Mn ion. On the other hand, the H43 mutation (MbF43H) was important for O–O bond cleavage, thereby leading to the high valent Mn-oxo intermediate (Figure 10B). This cooperative effect of

dual distal His residues resulted in a significant increase (up to 10-fold) in the reaction rate, compared to WT-Mn(III)-Mb.

More recently, in the oxone-mediated styrene epoxidation catalyzed by Mn(III)-Mb, Liu, Zhang and coworkers found that the simultaneous occurrence of three distal His residues (H64, H29 and H43) in the L29H/F43H mutant provided a remarkable increase in the reaction rate (8.9-fold increase compared to WT-Mn(III)-Mb).[100] The latter was hypothesized to rely on a synergic assistance of persulfate during O-O bond heterocleavage (Figure 11).

5b. Iron- and manganese-porphyrins housed within native non-metal containing protein scaffolds

To provide small-molecule chemical catalysts with second shell interactions and/or with a chiral environment, numerous researchers focused on the insertion of these systems into native protein scaffolds, which do not contain metal cofactors. Through this approach, several artificial enzymes have been developed that catalyze a variety of reactions, from oxidation reactions to C–C bond formation.[101,102] New artificial catalysts have been also developed through insertion of metalloporphyrins into macromolecular hosts. One useful approach is to raise antibodies against metalloporphyrins or ligand-modified metalloporphyrins, to enhance supramolecular association.

Along these lines, Mahy and coworkers developed "Hemoabzymes", artificial hemoproteins obtained raising monoclonal antibodies against differently substituted iron(III)-meso-tetra-phenyl porphyrins and MP8.[103] Their work on Fe(III)-α,α,α,β-mesotetrakis(ortho-carboxyphenyl)porphyrin, $\alpha_3\beta$-Fe(ToCPP), coupled with the recent

X-ray structural characterization of two systems,[104] allowed to carve out several aspects on the interaction between antibodies and synthetic porphyrins, and their implications on the catalysis. Hemoabzymes catalyzed the H_2O_2-mediated oxidation of a variety of co-substrates,[6] displaying a better peroxidase activity than Fe-porphyrins alone. This can be ascribed to the protective role of the protein, which prevents porphyrin oxidative self-degradation through π-stacking interactions. Hemoabzyme efficiency were far from their natural counterparts (k_{cat}/K_M values three to four orders of magnitude lower than those of peroxidases),[6] mainly for the lack of an axial ligand promoting the "push-effect" in H_2O_2 activation. MP8, bearing a His axial ligand for the iron (see Section 4) was used to solve this issue.[103] Indeed, the MP8-antibody complex, MP8-3A3,[103] is the best catalyst among Hemoabzymes, with a k_{cat}/K_M value only 2 orders of magnitude lower than HRP. This complex also showed enantioselectivity in thioether sulfoxidation (up to 45% *ee*).[105]

A different approach to insert synthetic porphyrin into a protein environment is the so-called "Trojan Horse" strategy.[106] It foresees the supramolecular association of a metalloporphyrin–ligand conjugate with a protein, which specifically binds that ligand. Mahy and coworkers applied this strategy for the development of their Hemozymes.[6] Taking advantage of the remarkable affinity of a monoclonal antibody for its estradiol antigen ($K_D = 9.5 \times 10^{-10}$ M), water-soluble Fe(III)- and Mn(III)-porphyrins (TMPyP: *meso*-tetrakis-(*p*-(*N*-methyl)-pyridiniumyl)-porphyrin or T*p*SPP: *meso*-tetrakis-(*p*-sulfonatophenyl)-porphyrin) were covalently modified with estradiol (Figure 12), and inserted into the anti-estradiol antibody 7A3.[106] In the H_2O_2-mediated sulfoxidation of thioanisole, both cationic (TMPyP) and anionic (T*p*SPP) iron-porphyrins were able to catalyze the chemoselective sulfoxidation of sulfides, with a small enantiomeric excess

(10%). The corresponding Mn(III)-containing porphyrins were inactive toward H_2O_2-mediated oxidations, whereas they catalyzed the $KHSO_5$-mediated epoxidation of styrene.[106] Conversion of the styrene was quantitative with the cationic Mn(III)-(TMPyP)-estradiol, while lower yields were observed with the anionic Mn(III)-(TpSPP)-estradiol. Interestingly, the presence of the protein did not increase the reaction yield for this reaction.

Following the "Trojan Horse" strategy, Fe(III)-T*p*SPP covalently modified with testosterone was inserted into a mutated form of the chromoprotein neocarzinostatin (NCS-3.24), known for its ability to strongly bind testosterone (K_D = 13 μM).[107] The resulting hemozyme catalyzed the chemoselective sulfoxidation of thioanisole by H_2O_2, even though with poor enantioselectivity (13% *ee*). Docking analysis (Figure xxx) proved that macrocycle-protein interactions, with the Fe(III)-porphyrin complex being sandwiched between two subdomains of the protein, account for the enhancement in testosterone binding (conjugate K_D value 1.6 μM).[108] A partial solvent exposure of the metal center could justify for the observed low enantioselectivity .

Hemozymes were also developed by the Mahy lab through the host-guest approach.[6] Anionic porphyrins were incorporated into the globally positive charged thermophilic β-1,4-endoxylanase or xylanase A (XlnA) from *Streptomyces lividans*.[109,110] Among a variety of anionic Fe(III)-porphyrins, only Fe(III)-(T*p*CPP) and Fe(III)-(T*p*SPP) (Figure 13) were able to tightly bind to XlnA, with K_D values in the micromolar range. Fe(III)-(T*p*CPP)–XlnA exibited a peroxidase activity and catalyzed the H_2O_2-mediated oxidation of guaiacol and *o*-dianisidine.[109] As observed in previous examples, XlnA had a protective role against the oxidative degradation of the porphyrin.[109] Fe(III)-(T*p*CPP)-

XlnA and Fe(III)-(T*p*SPP)-XlnA were able to catalyze the stereoselective oxidation of thioanisole. Significant improvement in chemical efficiency (85% yield, TOF: 1.09 min^{-1}) and increase in enantioselectivity (40% *ee*) was found when imidazole was added as co-catalyst (Figure 13).[111]

Replacement of iron with manganese allowed for the selective oxidation of aromatic alkenes.[110] Indeed, Mn(III)-(T*p*CPP)-XlnA catalyzed the epoxidation of styrene mediated by $KHSO_5$ (26% o.y., 17% yield for styrene oxide). Rather low chemo- and enantio-selectivities in favor of the (*S*)-isomer were observed in the epoxidation of unactivated alkenes (e.g. 4-chlorostyrene, 4-nitrostyrene) or poorly activated (e.g. 4-methylstyrene) alkenes. Conversely, the $KHSO_5$-mediated epoxidation of 4-methoxystyrene gave a higher overall yield (49.5%) and a higher and reversal enantioselectivity in the formation of styrene oxide (80% *ee* in favor of the (*R*)-isomer) (Figure 14A). Docking simulations suggested that during the reaction of styrene and its derivatives into the XlnA active site, the formation of the (*S*)-epoxide was energetically slightly favored (<0.5 kJ mol^{-1}). Conversely, the insertion of 4-methoxystyrene favors the formation of the (*R*)-epoxide (0.7 kJ mol^{-1}), owing to a stabilizing H-bond between Tyr 172 and the oxygen atom of 4-methoxy group (Figure 14B).[110]

Using a very simple procedure and thanks to the accessibility of a low-cost protein, Gross and coworkers used the host-guest approach to obtain artificial enzymes. They developed stereoselective metalloenzymes by mixing amphiphilic Fe- and Mn-corroles with various serum albumins (SAs).[112,113] Metal-corrole complexes bind HSA within a specific binding site, with a 1:1 stoichiometry, and with strong affinity (K_D in the micromolar range).[114] The resulting artificial SA-based metalloenzymes catalyzed the sulfoxidation of

thioanisole, and its derivatives, with conversions up to 98% and enantioselectivities up to 74%.[112,113] The utility of this simple and very efficient approach was demonstrated by the enantioselective synthesis of the pharmacologically important R-modafinil (better known as armodafinil), obtained by asymmetric sulfoxidation from its achiral precursor in 75% *ee* (Figure 15).

6. Beyond protein cages: metal-metalloporphyrin frameworks

As already shown in previous sections, protein and peptide-based heme-protein models have proven their ability to recapitulate some key features of enzymes. In the last years, the struggle to gain innovative and smart materials for industrial and technological applications has widened the field of protein design.[115–121] By means of supramolecular chemistry, it is now possible to build predictable composites of any desired size and shape.[122] Some of these fully synthetic materials do exhibit the inherent potential of enzyme catalysis. In this respect, MOFs can be seen as perfect candidates for the purpose of mimicking the structure-function relationship observed in natural proteins.[123]

MOFs are a class of crystalline materials containing organic linkers, or struts, interconnected by metal cations or metal clusters (nodes).[124] Their arrangement in the space gives rise to fascinating two- or three-dimensional networks. The variety of metallic nodes, linking struts, and the wide array of coordination geometries accounts for MOFs different structures and topology. Their tailorability, both in terms of size of channels and pores, as well as in terms of their physical and chemical properties makes them suitable for several applications.[125]

Many efforts have been devoted in altering and enhancing their properties, modifying their surface with appropriate decoration,[126] introducing functionality into the porous structure[127] or incorporating as struts molecules that have already revealed catalytic activity in homogeneous solution environments.[128] In this regard, the use of porphyrin molecules as bridging ligands is extremely attractive.[43,129–131] The incorporation of metalloporphyrin within MOF structures gives rise to new catalytic systems, which combine the activity of homogeneous catalysts with the robustness and recyclability of heterogeneous materials. The porphyrin-based MOFs, or metal-metalloporphyrin frameworks (MMPFs), show many advantages in terms of catalytic performance: (i) the MOF architecture preserves the catalytic centers from self-dimerization and oxidative degradation; (ii) the presence of large pockets greatly facilitates the substrate diffusion and confinement;[123] (iii) the catalytic activity can be modulated modifying either porphyrin substituents or the metal ion incorporated into the porphyrin ring, or the polarity of the binding pocket. The afforded metalloporphyrin framework should then feature high thermal, chemical, and water stabilities, thus meeting all of the prerequisites for a biomimetic system.

Over the past decades there has been an exponential growth in the synthesis of porphyrin-based MOFs,[132–134] though their applications in catalysis are still in the early stage. Nonetheless, few examples of heterogeneous biomimetic systems, proficient in oxidation reactions, present very promising properties. As a general trend, monoxygenation reactions have been performed in organic solvents, and the manganese is preferred over iron due to its higher reactivity and lower autoxidation under these conditions. When shifting to aqueous solvent, only peroxidase activity could be observed. In water,

oxygenating iron-catalysts would need an additional fifth ligand for modulating the electronic structure and the reduction potential, as in P450s.

The first catalytically porphyrin-based MOF was PIZA-3, a member of PIZA-n (Porphyrinic Illinois Zeolite Analogue) family, developed by Wilson and co-workers in 2005.[135] PIZA-3 consists of a Mn^{3+}-T*p*CPP linked by a trinuclear cluster of manganese(II). Its structure is characterized by pores of different size along the crystallographic *a* and *c* axes, creating an open framework with 56% void volume.

PIZA-3 was able of oxidizing linear and cyclic alkanes, and epoxidizing cyclic alkenes, using iodosylbenzene as oxidant. The oxidation activity was similar to other manganese porphyrins in homogeneous systems or immobilized on inorganic matrices as heterogeneous catalysts,[19] with the advantage that PIZA-3 can be simply recovered by filtration and reused for successive reactions.

Catalysis only occurred on the exterior surface of the crystalline material rather than inside the pores without any size- and shape-selectivities. The authors suggested that PIZA-3 pores were too small and hydrophilic to sorb nonpolar substrates within the framework. The prominent challenge would thus be the design of porphyrinic MOFs with more hydrophobic channels to improve the substrate diffusion.

Indeed, Wu and co-workers described a porous porphyrinic MOF, CZJ-1 (CZJ-Chemistry Department of Zhejiang University), with more hydrophobic channels.[136] CZJ-1 system was based on a manganese(III) T*p*CPP, an organic linker, N,N'-di-(4-pyridyl)-1,4,5,8- naphthalenetetracarboxydiimide, interconnected by a paddlewheel di-zinc cluster, linked together to generate the porous three-dimensional structure. CZJ-1 showed a flexibile structure that is also retained in desolvated conditions. It exhibited styrene and

cyclohexene epoxidation activity using iodosylbenzene as oxidant, and acetonitrile as solvent, at room temperature. CZJ-1 yielded a complete conversion of the substrates with 98% selectivity. The single-crystal X-ray structure of the styrene-included CZJ-1 demonstrated that the conversion of styrene occurs within the pores, thanks to the inclusion of the supporting organic linker (Figure 16). Finally, CZJ-1 reactivity was further tested towards the challenging oxidation of cyclohexane, observing a high catalytic activity in the oxidation of this substrate was observed, with a conversion up to 94%, and a high selectivity to the ketone.

One of the few active iron-porphyrin based MOFs in organic solvents was described by Zhou and co-workers.[137] PCN-221(Fe) catalyzed the monooxygenation of cyclohexane to cyclohexanol and cyclohexanone with a selectivity ratio of 5.4:86.9, using *tert*-butyl hydroperoxide as the oxidant. Only 18 turnovers were observed for this catalyst, highlighting the susceptibility of the iron porphyrin to autooxidation.

Despite the positive results above described, a true mimetic system of natural enzymes should be stable in water. It was therefore desirable to develop porphyrin-based MOFs stable in mixed aqueous/organic solvents, and lastly in water. The nature of the metal in the building blocks is crucial for the MOFs stability in water. Zinc(II) and copper(II), but in general divalent metal ions, show high water-exchange rate, which causes the framework decomposition. Therefore, harder metals that prefer the carboxylate ligands of the porphyrin should be adopted, and some chelating effect should be provided to increase the affinity of the terminal carboxylates.[138]

Chen, Wu and coworkers produced a system functioning in a mixed organic/aqueous solvent. They incorporated a *meso*-tetrakis-(3,5-dicarboxylphenyl)porphyrin into porous

MOFs, developing three materials: ZJU-18, ZJU-19 and ZJU-20 (ZJU—Zheijang University).[139] The three compounds differed for the metal ion, both in the porphyrin ring and in the clusters (manganese porphyrin and manganese clusters for ZJU-18 (Figure 17), nickel porphyrins and manganese clusters for ZJU-19, manganese porphyrin and cadmium clusters for ZJU-20). X-ray analysis revealed that these MOFs are isomorphous. They are characterized by large cavities and pore windows, with the metalloporphyrins accessible to solvent and substrates. These three compounds were tested for the peroxygenation of ethylbenzene to acetophenone, performed in a mixed solvent of acetonitrile, acetic acid and water, at 65°C, using tert-butyl hydroperoxide as the oxidant. ZJU-18 led to quantitative conversion of the substrate, while ZJU-19 is able to convert only 9% of ethylbenzene, demonstrating the catalytic role of the manganese porphyrin in the oxidation. The other hand, the manganese involved in the bridging clusters is also catalytically active, considering the lower activity of ZJU-20 compared to ZJU-18. Finally, ZJU-18 showed the following features: (i) easy recovery by centrifugation and subsequently reusable for 15 cycles; (ii) the catalytic oxidation of ethylbenzene into acetophenone does occur inside the pores (substrate confinement); (iii) product release mechanism, by different affinity between substrate and product; (iv) size- and shape-selectivity, as the substrate conversion gradually decreased as the size of the substrate increases.

Zhou and co-workers developed the first iron-based MMPF active in aqueous buffer. They prepared a zirconium-porphyrinic MOF, called PCN-222 (Fe), similar to its predecessor PCN221 (Fe), but stable in water.[140] Interestingly, its peroxidase reactivity follows the conventional Michaelis–Menten saturation kinetics. This framework is made

up of the water stable Zr_6 octahedron cluster linked to eight Fe^{3+}-T*p*CPP. In the three-dimensional structure two types of pores were observed, assigned to as trigonal micro-channels and hexagonal meso-channels. PCN-222 (Fe) was employed in the oxidation of several substrates, including pyrogallol, 3,3,5,5-tetromethylbenzidine and *o*-phenyldiamine, remarkably using hydrogen peroxide as the oxidant. Though, PCN-222 showed enhanced activity compared to the free hemin, a worse catalytic efficiency than horseradish peroxidase was observed. Intriguingly, the K_M values are comparable, which indicates that the affinity to the substrates is similar for the two systems.

Motivated by the previous encouraging results, Zhou and coworkers tried to adopt the abundant and non-toxic iron even for the nodal clusters.[141] Though, PCN-600 (Fe) exhibited saturation kinetics as its predecessor, unfortunately with lower catalytic parameters. We may speculate that side reactivity of the iron clusters could explain the different behaviors of the two systems though.

Ma's group has been developing a family of MMPFs, characterized by carboxyphenyl-substituted metalloporphyrins.[142] The porphyrins are linked together by different metal clusters (Cu, Co, Zn, Cd, Zr, Fe) coordinated by the porphyrin carboxyl groups without any additional linker. Among the members of this family, as previously observed, the zirconium-based MMPF-6 is of great interest for its bio-mimicking activity, as it is stable in water. An active iron(III) is pentacoordinated by the tetrakis(p-carboxyphenyl)porphyrin and a chloride anion. Single crystal X-ray studies demonstrated that the three-dimensional structure consists of hexagonal and trigonal channels in which Fe-T*p*CPP-Cl are oriented towards the channels and connected by $Zr_6O_8(carboxy)_8(H_2O)_8$. MMPF-6 peroxidase activity was assessed by two standard

assays: the oxidation of pyrogallol to purpurogallin and of ABTS in HEPES buffer and compared to the natural myoglobin (Figure 18). Although peroxidase activity of myoglobin has been widely studied, its natural role is dioxygen binding and not hydrogen peroxide activation, making difficult to accurately evaluate the results. MMPF-6 shows a noteworthy activity in oxidation and electron transfer mechanisms, with an initial rate only three to four times lower than free myoglobin, respectively. The initial rate for MMPF-6 is probably slowed down by scarce diffusion of the substrates into the channels. MMPF-6 can be reused up to 4 times without loss of activity, and can operate in ethanol, which may cause protein denaturation.

In conclusion, MOFs are nowadays an emerging field in the discovery of new solid-state platforms for nature biomimicking. Advances in MOF research make them more and more attractive tools for catalysis. Compared to zeolites, resins etc., MOF offer a stable and organized skeleton that ensures constant environment to the catalytic active site and can efficiently tune enzyme-like activity. Finally, an ordered arrangement of channels or pores in MOFs enables efficient diffusion of reactants, their conversion into products and their fast exchange with bulk solution. Moreover, MOFs activity can be oriented towards selectivity by tuning the channel environment. However, a deeper spectroscopic study on the catalytic intermediates would be necessary to gain new insight for developing porphyrin-based MOFs approaching the catalytic efficiency of the natural counterparts.

7. Concluding remarks

The examples described in this review illustrate the remarkable progress reached in the last two decades in developing heme-enzyme mimics, active in oxidation catalysis.

Different approaches of protein design and re-designed have allowed the construction of more and more elaborate enzyme-like architecture around the metalloporphyrins, which hold increasingly impressive catalytic efficiencies. This is particular evident in those models, mimicking peroxidase activity, as illustrated in Table 1. Further advancement of the field would require developing artificial metalloenzymes, able to use the bioavailable and inexpensive O_2 as the oxidant. Toward this goal, directed evolution, recently reviewed by us,[8] has being demonstrating a valuable approach, which can complement rational design. A remarkable result was achieved by Arnold and coworker: by directed evolution of a cytochrome P450 enzyme, they obtained a selective alkene anti-Markovnikov oxygenase that uses dioxygen as the terminal oxidant.[143]

Directed evolution, through an iterative process of protein mutation and screening for activity, allows identifying amino acid substitutions required for an enzyme to perform a desired function. However, it do not test our understanding in structural-function relationship, and, as consequence, do not allow the developed of small/medium sized enzymes that encompass the minimal requirements for function.

We believe that scientists should treasure all the lessons learned from the different strategies, in order to exceed the results gained so far. This will open, in a near future, new opportunities for the construction of better performing catalysts, based on metalloporphyrins caged in different natural and/or synthetic scaffolds. Such catalysts would have an important economic and social impact, as a very broad spectrum of processes has to benefit of "greener" catalysts for a sustainable future: hydrocarbon conversion, oxidative decontamination of industrial wastes, stereoselective synthesis in pharmaceutical industry.[6]

8. Acknowledgements

We wish to thank all former members of our group for their contributions to the results described in this review, and Fabrizia Sibillo for help in the final editing of the manuscript. The work from authors' groups reported herein has been supported by European Union (EU) (Cost Action CM1003 - Biological Oxidation Reactions: Mechanisms and Design of New Catalysts) and the Scientific Research Department of Campania Region (BIP Project, POR FESR 2007/2013, grant number B25C13000290007).

9. Dedication

This article is dedicated to Vincenzo Pavone on the occasion of his 65th birthday. His ceaseless effort, enthusiasm and thoroughness in doing Science, and in teaching, has been and still is a source of great inspiration to all of us and to all his students.

10. References

1. Lombardi, A.; Nastri, F.; Pavone, V. Chem Rev 2001, 101, 3165–3189.
2. Reedy, C. J.; Gibney, B. R. Chem Rev 2004, 104, 617–650.
3. Watanabe, Y.; Nakajima, H.; Ueno, T. Acc Chem Res 2007, 40, 554–562.
4. Yu, F.; Cangelosi, V. M.; Zastrow, M. L.; Tegoni, M.; Plegaria, J. S.; Tebo, A. G.; Mocny, C. S.; Ruckthong, L.; Qayyum, H.; Pecoraro, V. L. Chem Rev 2014, 114, 3495–3578.
5. Petrik, I. D.; Liu, J.; Lu, Y. Curr Opin Chem Biol 2014, 19, 67–75.
6. Mahy, J.-P.; Maréchal, J.-D.; Ricoux, R. Chem Commun 2015, 51, 2476–2494.
7. Oohora, K.; Hayashi, T. Methods in Enzymology; Peptide, Protein and Enzyme Design; Academic Press, 2016; Vol. 580; pp 439–454.
8. Nastri, F.; Chino, M.; Maglio, O.; Bhagi-Damodaran, A.; Lu, Y.; Lombardi, A. Chem Soc Rev 2016, 45, 5020–5054.
9. Schwizer, F.; Okamoto, Y.; Heinisch, T.; Gu, Y.; Pellizzoni, M. M.; Lebrun, V.; Reuter, R.; Köhler, V.; Lewis, J. C.; Ward, T. R. Chem Rev 2017, 10.1021/acs.chemrev.7b00014.
10. Wolfenden, R.; Snider, M. J. Acc Chem Res 2001, 34, 938–945.
11. Ortiz de Montellano, P. R. Cytochrome P450 - Structure, Mechanism and Biochemistry; Springer International Publishing: Switzerland, 2005.
12. Matsui, T.; Unno, M.; Ikeda-Saito, M. Acc Chem Res 2010, 43, 240–247.
13. Raven, E.; Dunford, B. Heme Peroxidases; Metallobiology; The Royal Society of Chemistry: Cambridge, 2016.
14. Kaila, V. R. I.; Verkhovsky, M. I.; Wikström, M. Chem Rev 2010, 110, 7062–7081.
15. Hino, T.; Matsumoto, Y.; Nagano, S.; Sugimoto, H.; Fukumori, Y.; Murata, T.; Iwata, S.; Shiro, Y. Science 2010, 330, 1666–1670.
16. Groves, J. T.; Wang, C. C.-Y. Curr Opin Chem Biol 2000, 4, 687–695.
17. Maglio, O.; Nastri, F.; Lombardi, A. Ionic Interactions in Natural and Synthetic Macromolecules; John Wiley & Sons, Inc.: Hoboken, NJ, USA, 2012; pp 361–450.
18. Friedle, S.; Reisner, E.; Lippard, S. J. Chem Soc Rev 2010, 39, 2768–2779.
19. Costas, M. Coord Chem Rev 2011, 255, 2912–2932.

20. Lichtenstein, B. R.; Farid, T. A.; Kodali, G.; Solomon, L. A.; Anderson, J. L. R.; Sheehan, M. M.; Ennist, N. M.; Fry, B. A.; Chobot, S. E.; Bialas, C.; Mancini, J. A.; Armstrong, C. T.; Zhao, Z.; Esipova, T. V.; Snell, D.; Vinogradov, S. A.; Discher, B. M.; Moser, C. C.; Dutton, P. L. Biochem Soc Trans 2012, 40, 561–566.

21. Oloo, W. N.; Que Jr., L. Comprehensive Inorganic Chemistry II (Second Edition); Elsevier: Amsterdam, 2013; pp 763–778.

22. Lewis, J. C. ACS Catal 2013, 3, 2954–2975.

23. Lee, S. C.; Lo, W.; Holm, R. H. Chem Rev 2014, 114, 3579–3600.

24. Chino, M.; Maglio, O.; Nastri, F.; Pavone, V.; DeGrado, W. F.; Lombardi, A. Eur J Inorg Chem 2015, 2015, 3371–3390.

25. Caserta, G.; Roy, S.; Atta, M.; Artero, V.; Fontecave, M. Curr Opin Chem Biol 2015, 25, 36–47.

26. Itoh, S. Acc Chem Res 2015, 48, 2066–2074.

27. Bhagi-Damodaran, A.; Petrik, I.; Lu, Y. Isr J Chem 2016, 56, 773–790.

28. Lin, Y.-W. Coord Chem Rev 2017, 336, 1–27.

29. Bren, K. L. J Am Chem Soc 2017, 139, 14331–14334.

30. Reig, A. J.; Pires, M. M.; Snyder, R. A.; Wu, Y.; Jo, H.; Kulp, D. W.; Butch, S. E.; Calhoun, J. R.; Szyperski, T.; Solomon, E. I.; DeGrado, W. F. Nat Chem 2012, 4, 900–906.

31. Faiella, M.; Andreozzi, C.; de Rosales, R. T. M.; Pavone, V.; Maglio, O.; Nastri, F.; DeGrado, W. F.; Lombardi, A. Nat Chem Biol 2009, 5, 882–884.

32. Cangelosi, V. M.; Deb, A.; Penner-Hahn, J. E.; Pecoraro, V. L. Angew Chem Int Ed 2014, 53, 7900–7903.

33. Yu, Y.; Cui, C.; Liu, X.; Petrik, I. D.; Wang, J.; Lu, Y. J Am Chem Soc 2015, 137, 11570–11573.

34. Watkins, D. W.; Jenkins, J. M. X.; Grayson, K. J.; Wood, N.; Steventon, J. W.; Vay, K. K. L.; Goodwin, M. I.; Mullen, A. S.; Bailey, H. J.; Crump, M. P.; MacMillan, F.; Mulholland, A. J.; Cameron, G.; Sessions, R. B.; Mann, S.; Anderson, J. L. R. Nat Commun 2017, 8, 358.

35. Chino, M.; Leone, L.; Maglio, O.; D'Alonzo, D.; Pirro, F.; Pavone, V.; Nastri, F.; Lombardi, A. Angew Chem Int Ed 2017, 10.1002/anie.201707637.

36. Liu, W.; Groves, J. T. Acc Chem Res 2015, 48, 1727–1735.

37. Che, C.-M.; Lo, V. K.-Y.; Zhou, C.-Y.; Huang, J.-S. Chem Soc Rev 2011, 40, 1950–1975.

38. Baglia, R. A.; Zaragoza, J. P. T.; Goldberg, D. P. Chem Rev 2017, 10.1021/acs.chemrev.7b00180.

39. Beletskaya, I.; Tyurin, V. S.; Tsivadze, A. Y.; Guilard, R.; Stern, C. Chem Rev 2009, 109, 1659–1713.

40. Drain, C. M.; Varotto, A.; Radivojevic, I. Chem Rev 2009, 109, 1630–1658.

41. Stulz, E. Acc Chem Res 2017, 50, 823–831.

42. Raynal, M.; Ballester, P.; Vidal-Ferran, A.; van Leeuwen, P. W. N. M. Chem Soc Rev 2014, 43, 1734–1787.

43. Gao, W.-Y.; Chrzanowski, M.; Ma, S. Chem Soc Rev 2014, 43, 5841–5866.

44. Helm, L.; Merbach, A. E. Chem Rev 2005, 105, 1923–1960.

45. Bertini, I. Biological Inorganic Chemistry: Structure and Reactivity; University Science Books: Maplewood, New Jersey (USA), 2007.

46. Buchler, J.W. The Porphyrins, Volume 1; NY, USA, 1979; Vol. I; pp 389–483.

47. Najafpour, M. M.; Renger, G.; Hołyńska, M.; Moghaddam, A. N.; Aro, E.-M.; Carpentier, R.; Nishihara, H.; Eaton-Rye, J. J.; Shen, J.-R.; Allakhverdiev, S. I. Chem Rev 2016, 116, 2886–2936.

48. Haynes, W. M. CRC handbook of chemistry and physics; CRC press: Boca Raton, FL (USA), 2014.

49. Liu, J.; Chakraborty, S.; Hosseinzadeh, P.; Yu, Y.; Tian, S.; Petrik, I.; Bhagi, A.; Lu, Y. Chem Rev 2014, 114, 4366–4469.

50. Batinic-Haberle, I.; Tovmasyan, A.; Spasojevic, I. Redox Biol 2015, 5, 43–65.

51. Poulos, T. L. Chem Rev 2014, 114, 3919–3962.

52. Perutz, M. F.; Wilkinson, A. J.; Paoli, M.; Dodson, G. G. Annu Rev Biophys Biomol Struct 1998, 27, 1–34.

53. Taniguchi, I.; Watanabe, K.; Tominaga, M.; Hawkridge, F. M. J Electroanal Chem 1992, 333, 331–338.

54. Taniguchi, I.; Li, C.; Ishida, M.; Yao, Q. J Electroanal Chem 1999, 460, 245–250.

55. Fürstner, A. ACS Cent Sci 2016, 2, 778–789.

56. Meunier, B.; de Visser, S. P.; Shaik, S. Chem Rev 2004, 104, 3947–3980.

57. Mondal, M. S.; Mitra, S. Biochim Biophys Acta Protein Struct Mol Enzymol 1996, 1296, 174–180.

58. Hiner, A. N. P.; Hernández-Ruiz, J.; Williams, G. A.; Arnao, M. B.; García-Cánovas, F.; Acosta, M. Arch Biochem Biophys 2001, 392, 295–302.

59. Campomanes, P.; Rothlisberger, U.; Alfonso-Prieto, M.; Rovira, C. J Am Chem Soc 2015, 137, 11170–11178.

60. Kumar, D.; Visser, S. P. de; Sharma, P. K.; Derat, E.; Shaik, S. J Biol Inorg Chem 2005, 10, 181–189.

61. Wang, X.; Peter, S.; Ullrich, R.; Hofrichter, M.; Groves, J. T. Angew Chem Int Ed 2013, 52, 9238–9241.

62. Giuntini, F.; A. Alonso, C. M.; W. Boyle, R. Photochem Photobiol Sci 2011, 10, 759–791.

63. Ladomenou, K.; Nikolaou, V.; Charalambidis, G.; Coutsolelos, A. G. Coord Chem Rev 2016, 306, 1–42.

64. Iranzo, O. Bioorganic Chem 2011, 39, 73–87.

65. Asayama, S.; Mori, T.; Nagaoka, S.; Kawakami, H. J Biomater Sci Polym Ed 2003, 14, 1169–1179.

66. Asayama, S.; Kawamura, E.; Nagaoka, S.; Kawakami, H. Mol Pharm 2006, 3, 468–470.

67. Umezawa, N.; Matsumoto, N.; Iwama, S.; Kato, N.; Higuchi, T. Bioorg Med Chem 2010, 18, 6340–6350.

68. Watanabe, Y.; Namba, A.; Umezawa, N.; Kawahata, M.; Yamaguchi, K.; Higuchi, T. Chem Commun 2006, 4958–4960.

69. Marques, H. M. Dalton Trans 2007, 4371–4385.

70. Boersma, M. G.; Primus, J.-L.; Koerts, J.; Veeger, C.; Rietjens, I. M. C. M. Eur J Biochem 2000, 267, 6673–6678.

71. Kadnikova, E. N.; Kostić, N. M. J Org Chem 2003, 68, 2600–2608.

72. Dallacosta, C.; Monzani, E.; Casella, L. J Biol Inorg Chem 2003, 8, 770–776.

73. Dallacosta, C.; Casella, L.; Monzani, E. ChemBioChem 2004, 5, 1692–1699.

74. Primus, J.-L.; Boersma, M. G.; Mandon, D.; Boeren, S.; Veeger, C.; Weiss, R.; Rietjens, I. M. C. M. J Biol Inorg Chem 1999, 4, 274–283.

75. Primus, J.-L.; Grunenwald, S.; Hagedoorn, P.-L.; Albrecht-Gary, A.-M.; Mandon, D.; Veeger, C. J Am Chem Soc 2002, 124, 1214–1221.

76. Veeger, C. J Inorg Biochem 2002, 91, 35–45.

77. Lombardi, A.; Nastri, F.; Marasco, D.; Maglio, O.; De Sanctis, G.; Sinibaldi, F.; Santucci, R.; Coletta, M.; Pavone, V. Chem - Eur J 2003, 9, 5643–5654.

78. Di Costanzo, L.; Geremia, S.; Randaccio, L.; Nastri, F.; Maglio, O.; Lombardi, A.; Pavone, V. J Biol Inorg Chem 2004, 9, 1017–1027.

79. Nastri, F.; Lista, L.; Ringhieri, P.; Vitale, R.; Faiella, M.; Andreozzi, C.; Travascio, P.; Maglio, O.; Lombardi, A.; Pavone, V. Chem - Eur J 2011, 17, 4444–4453.

80. Vitale, R.; Lista, L.; Cerrone, C.; Caserta, G.; Chino, M.; Maglio, O.; Nastri, F.; Pavone, V.; Lombardi, A. Org Biomol Chem 2015.

81. Venanzi, M.; Cianfanelli, S.; Palleschi, A. J Pept Sci 2014, 20, 36–45.

82. Nastri, F.; Bruni, R.; Maglio, O.; Lombardi, A. Coordination Chemistry in Protein Cages; John Wiley & Sons, Inc.: Hoboken, NJ (USA), 2013; pp 43–85.

83. Faiella, M.; Maglio, O.; Nastri, F.; Lombardi, A.; Lista, L.; Hagen, W. R.; Pavone, V. Chem – Eur J 2012, 18, 15960–15971.

84. Frolow, F.; Kalb, A. J.; Yariv, J. Nat Struct Mol Biol 1994, 1, 453–460.

85. Farid, T. A.; Kodali, G.; Solomon, L. A.; Lichtenstein, B. R.; Sheehan, M. M.; Fry, B. A.; Bialas, C.; Ennist, N. M.; Siedlecki, J. A.; Zhao, Z.; Stetz, M. A.; Valentine, K. G.; Anderson, J. L. R.; Wand, A. J.; Discher, B. M.; Moser, C. C.; Dutton, P. L. Nat Chem Biol 2013, 9, 826–833.

86. Koder, R. L.; Anderson, J. L. R.; Solomon, L. A.; Reddy, K. S.; Moser, C. C.; Dutton, P. L. Nature 2009, 458, 305–309.

87. Anderson, J. L. R.; Armstrong, C. T.; Kodali, G.; Lichtenstein, B. R.; Watkins, D. W.; Mancini, J. A.; Boyle, A. L.; Farid, T. A.; Crump, M. P.; Moser, C. C.; Dutton, P. L. Chem Sci 2014, 5, 507–514.

88. Hayashi, T. Coordination Chemistry in Protein Cages; John Wiley & Sons, Inc.: Hoboken, NJ (USA), 2013; pp 87–110.

89. Kleingardner, J. G.; Bren, K. L. Acc Chem Res 2015, 48, 1845–1852.

90. Hayashi, T.; Dejima, H.; Matsuo, T.; Sato, H.; Murata, D.; Hisaeda, Y. J Am Chem Soc 2002, 124, 11226–11227.

91. Hayashi, T.; Murata, D.; Makino, M.; Sugimoto, H.; Matsuo, T.; Sato, H.; Shiro, Y.; Hisaeda, Y. Inorg Chem 2006, 45, 10530–10536.

92. Matsuo, T.; Murata, D.; Hisaeda, Y.; Hori, H.; Hayashi, T. J Am Chem Soc 2007, 129, 12906–12907.

93. Matsuo, T.; Hayashi, A.; Abe, M.; Matsuda, T.; Hisaeda, Y.; Hayashi, T. J Am Chem Soc 2009, 131, 15124–15125.

94. Hayashi, T.; Hisaeda, Y. Acc Chem Res 2002, 35, 35–43.

95. Matsuo, T.; Fukumoto, K.; Watanabe, T.; Hayashi, T. Chem – Asian J 2011, 6, 2491–2499.

96. Oohora, K.; Kihira, Y.; Mizohata, E.; Inoue, T.; Hayashi, T. J Am Chem Soc 2013, 135, 17282–17285.

97. Cai, Y.-B.; Li, X.-H.; Jing, J.; Zhang, J.-L. Metallomics 2013, 5, 828–835.

98. Zahran, Z. N.; Chooback, L.; Copeland, D. M.; West, A. H.; Richter-Addo, G. B. J Inorg Biochem 2008, 102, 216–233.

99. Stone, K. L.; Hua, J.; Choudhry, H. Inorganics 2015, 3, 219–229.

100. Cai, Y.-B.; Yao, S.-Y.; Hu, M.; Liu, X.; Zhang, J.-L. Inorg Chem Front 2016, 3, 1236–1244.

101. Hamels, D. R.; Ward, T. R. Comprehensive Inorganic Chemistry II (Second Edition); Elsevier: Amsterdam, 2013; pp 737–761.

102. Steinreiber, J.; Ward, T. R. Coord Chem Rev 2008, 252, 751–766.

103. Ricoux, R.; Sauriat-Dorizon, H.; Girgenti, E.; Blanchard, D.; Mahy, J.-P. J Immunol Methods 2002, 269, 39–57.

104. Robles, V. M.; Maréchal, J.-D.; Bahloul, A.; Sari, M.-A.; Mahy, J.-P.; Golinelli-Pimpaneau, B. PLOS ONE 2012, 7, e51128.

105. Ricoux, R.; Lukowska, E.; Pezzotti, F.; Mahy, J.-P. Eur J Biochem 2004, 271, 1277–1283.

106. Sansiaume, E.; Ricoux, R.; Gori, D.; Mahy, J.-P. Tetrahedron Asymmetry 2010, 21, 1593–1600.

107. Drevelle, A.; Graille, M.; Heyd, B.; Sorel, I.; Ulryck, N.; Pecorari, F.; Desmadril, M.; van Tilbeurgh, H.; Minard, P. J Mol Biol 2006, 358, 455–471.

108. Sansiaume-Dagousset, E.; Urvoas, A.; Chelly, K.; Ghattas, W.; Maréchal, J.-D.; Mahy, J.-P.; Ricoux, R. Dalton Trans 2014, 43, 8344–8354.

109. Ricoux, R.; Dubuc, R.; Dupont, C.; Marechal, J.-D.; Martin, A.; Sellier, M.; Mahy, J.-P. Bioconjug Chem 2008, 19, 899–910.

110. Allard, M.; Dupont, C.; Muñoz Robles, V.; Doucet, N.; Lledós, A.; Maréchal, J.-D.; Urvoas, A.; Mahy, J.-P.; Ricoux, R. ChemBioChem 2012, 13, 240–251.

111. Ricoux, R.; Allard, M.; Dubuc, R.; Dupont, C.; Maréchal, J.-D.; Mahy, J.-P. Org Biomol Chem 2009, 7, 3208–3211.

112. Mahammed, A.; Gross, Z. J Am Chem Soc 2005, 127, 2883–2887.

113. Nigel-Etinger, I.; Mahammed, A.; Gross, Z. Catal Sci Technol 2011, 1, 578–581.

114. Mahammed, A.; Gray, H. B.; Weaver, J. J.; Sorasaenee, K.; Gross, Z. Bioconjug Chem 2004, 15, 738–746.

115. Grigoryan, G.; Kim, Y. H.; Acharya, R.; Axelrod, K.; Jain, R. M.; Willis, L.; Drndic, M.; Kikkawa, J. M.; Degrado, W. F. Science 2011, 332, 1071–1076.

116. King, N. P.; Bale, J. B.; Sheffler, W.; McNamara, D. E.; Gonen, S.; Gonen, T.; Yeates, T. O.; Baker, D. Nature 2014, 510, 103–108.

117. Rufo, C. M.; Moroz, Y. S.; Moroz, O. V.; Stöhr, J.; Smith, T. A.; Hu, X.; DeGrado, W. F.; Korendovych, I. V. Nat Chem 2014, 6, 303–309.

118. Gonen, S.; DiMaio, F.; Gonen, T.; Baker, D. Science 2015, 348, 1365–1368.

119. Kaltofen, S.; Li, C.; Huang, P.-S.; Serpell, L. C.; Barth, A.; André, I. J Mol Biol 2015, 427, 550–562.

120. Kim, K.-H.; Ko, D.-K.; Kim, Y.-T.; Kim, N. H.; Paul, J.; Zhang, S.-Q.; Murray, C. B.; Acharya, R.; DeGrado, W. F.; Kim, Y. H.; Grigoryan, G. Nat Commun 2016, 7, ncomms11429.

121. Suzuki, Y.; Cardone, G.; Restrepo, D.; Zavattieri, P. D.; Baker, T. S.; Tezcan, F. A. Nature 2016, 533, 369–373.

122. Lin, Y.; Mao, C. Front Mater Sci 2011, 5, 247–265.

123. Nath, I.; Chakraborty, J.; Verpoort, F. Chem Soc Rev 2016, 45, 4127–4170.

124. James, S. L. Chem Soc Rev 2003, 32, 276–288.

125. Furukawa, H.; Cordova, K. E.; O'Keeffe, M.; Yaghi, O. M. Science 2013, 341, 1230444.

126. McGuire, C. V.; Forgan, R. S. Chem Commun 2015, 51, 5199–5217.

127. Larsen, R. W.; Wojtas, L.; Perman, J.; Musselman, R. L.; Zaworotko, M. J.; Vetromile, C. M. J Am Chem Soc 2011, 133, 10356–10359.

128. Das, M. C.; Xiang, S.; Zhang, Z.; Chen, B. Angew Chem Int Ed 2011, 50, 10510–10520.

129. Nakagaki, S.; Ferreira, G.; Ucoski, G.; Dias de Freitas Castro, K. Molecules 2013, 18, 7279–7308.

130. Guo, Z.; Chen, B. Dalton Trans 2015, 44, 14574–14583.

131. Pereira, C.; Simões, M.; Tomé, J.; Almeida Paz, F. Molecules 2016, 21, 1348.

132. Abrahams, B. F.; Hoskins, B. F.; Michail, D. M.; Robson, R. Nature 1994, 369, 727–729.

133. Goldberg, I. Chem – Eur J 2000, 6, 3863–3870.

134. Kosal, M. E.; Chou, J.-H.; Wilson, S. R.; Suslick, K. S. Nat Mater 2002, 1, 118–121.

135. Suslick, K. S.; Bhyrappa, P.; Chou, J.-H.; Kosal, M. E.; Nakagaki, S.; Smithenry, D. W.; Wilson, S. R. Acc Chem Res 2005, 38, 283–291.

136. Xie, M.-H.; Yang, X.-L.; He, Y.; Zhang, J.; Chen, B.; Wu, C.-D. Chem – Eur J 2013, 19, 14316–14321.

137. Feng, D.; Jiang, H.-L.; Chen, Y.-P.; Gu, Z.-Y.; Wei, Z.; Zhou, H.-C. Inorg Chem 2013, 52, 12661–12667.

138. Gu, Z.-Y.; Park, J.; Raiff, A.; Wei, Z.; Zhou, H.-C. ChemCatChem 2014, 6, 67–75.

139. Yang, X.-L.; Xie, M.-H.; Zou, C.; He, Y.; Chen, B.; O'Keeffe, M.; Wu, C.-D. J Am Chem Soc 2012, 134, 10638–10645.

140. Feng, D.; Gu, Z.-Y.; Li, J.-R.; Jiang, H.-L.; Wei, Z.; Zhou, H.-C. Angew Chem Int Ed 2012, 51, 10307–10310.

141. Wang, K.; Feng, D.; Liu, T.-F.; Su, J.; Yuan, S.; Chen, Y.-P.; Bosch, M.; Zou, X.; Zhou, H.-C. J Am Chem Soc 2014, 136, 13983–13986.

142. Chen, Y.; Hoang, T.; Ma, S. Inorg Chem 2012, 51, 12600–12602.

143. Hammer, S. C.; Kubik, G.; Watkins, E.; Huang, S.; Minges, H.; Arnold, F. H. Science 2017, 358, 215–218.

144. Schrödinger, L. L. C. The PyMOL Molecular Graphics System, Version 1.3r1, 2010.

Figure Legends

Figure 1. Designed or engineered enzyme-like cages classification. Schematic representation of (A) Covalent systems: short peptides or protein are covalently bound to the metal cofactor; (B) Non-covalent systems: the protein scaffold, represented as a chest, can be opportunely functionalized/"filled" with porphyrinoid rings by *i)* cofactor replacement, or *ii)* cofactor incorporation; (C) Metal-metalloporphyrin frameworks: a metal cluster node, represented as a blue prism, interconnects several metalloporphyrins, generating two- or three-dimensional lattices.

Figure 2. Heme paradigm for oxidation. Schematic representation of the different intermediates generated during the four different reaction pathways: superoxide dismutation (pink), peroxide dismutation (green), oxidase/peroxidase (blue), oxygenase/peroxygenase (red). Peroxide shunt, which allows bypassing the two reductive steps needed to activate dioxygen, is depicted as a black arrow.

Figure 3. (A) Mn-porphyrin–catalase conjugate with the dual function of SOD and catalase; (B) Mn-porphyrin-oligopeptide conjugate with SOD activity.

Figure 4. Microperoxidases and their catalyzed oxidation reactions.

Figure 5. Miniaturized heme-proteins. Molecular models of: (A) E2L(TD)-Fe(III)-mimochrome VI with key residues depicted as sticks: the coordinating His6, the hydrophobic Leu2 at N-terminal position and the catalytic Arg10 on the distal site; (B) Fe(III)-MP3 with key residues of the first and second coordination spheres depicted as sticks: the His32 and the hydrogen-bonded Asp9 on the proximal site, the catalytic Arg13 on the distal site. The structures were generated using PyMol.[144]

Figure 6. Design strategy for C-type cytochrome maquettes (CTMs). Adapted from ref. 34.

Figure 7. Native Fe(III)-protoporphyrin IX (Fe-PPIX) and the synthetic Fe(III)-porphycene (Fe-Pc) and Fe(III)-corrole (Fe-Cor).

Figure 8. "Single winged" synthetic cofactor used in reconstitution of MbH64D.

Figure 9. (A) Mn(III)-Pc cofactor used in reconstitution of Mb; (B) Hydroxylation of ethylbenzene catalyzed by Mn(III)-Pc-Mb. Adapted with permission from ref. 96. Copyright 2013 American Chemical Society.

Figure 10. Mechanism of Mn(IV)=O intermediate formation in (A) Mn(III)-wtMb, assisted by distal histidine at the position 64, and in (B) Mn(III)-F43H-Mb mutant, assisted by two distal histidines at positions 64 and 43. Adapted with permission from ref. 97. Copyright 2013 RSC.

Figure 11. Oxone-mediated styrene epoxidation, through synergic assistance of His64, His29 and His43 residues, in the Mn(III)-L29H/F43H-Mb mutant. Adapted with permission from ref. 100. Copyright 2016 RSC.

Figure 12. (A) Structure of metalloporphyrin-estradiol conjugates. (B) Docking model of Fe(III)-T*p*SPP-testosterone complexed with neocarzinostatin variant, NCS-3.24. Adapted with permission from ref. 6. Copyright 2015 RSC.

Figure 13. Fe(III)- and Mn(III)-porphyrins used in complex with Xln10A.

Figure 14. (A) Reaction scheme of styrene oxidation catalyzed by Mn-(T*p*CPP)-Xln10A enzyme, with the total yields in the oxidation products; (B) Docking model of *p*-methoxystyrene in the metallo-enzyme. Styrene orientation is consistent with *R*-epoxide formation. Adapted with permission from ref. 110. Copyright Wiley 2012.

Figure 15. (A) Structure of Mn(III)-corrole catalyst for sulfoxidation reaction; (B) Reaction scheme of the asymmetric synthesis of Armodafinil.

Figure 16. Crystal structures of (A) CZJ-1 (CCDC: 923792) and (B) styrene-included CZJ-1 (CCDC: 882227) viewed along the channels. Adapted with permission from ref. 136. Copyright 2013 Wiley.

Figure 17. Crystal structure of ZJU-18 (CCDC: 898632). Mn(III)-*meso*-tetrakis-(3,5-dicarboxylphenyl)porphyrin connected to binuclear $Mn_2(COO)_4$ and trinuclear $Mn_3(COO)_4(\mu\text{-}H_2O)_2$ units. The Mn-centered polyhedra are shown in different shades of blue. Reprinted with permission from ref. 139. Copyright 2012 American Chemical Society.

Figure 18. Biomimetic catalyst MMPF-6. Fe(III)-T*p*CPP-Cl connected with zirconium oxide clusters demonstrated peroxidase activity comparable to the natural myoglobin. Reprinted with permission from ref. 142. Copyright 2012 American Chemical Society.

Table 1. Comparison of the catalytic efficiency for H_2O_2-dependent oxidation of selected co-substrates by natural HRP and heme-protein models.

Catalyst	Substrate	pH	k_{cat}/K_M [M^{-1} min^{-1}]	References
HRP	**ABTS**	4.6	5.8×10^6	31
HRP	**ABTS**	7.0	1.03×10^4	31
C45	**ABTS**	8.58	3.2×10^6	34
Fe^{3+}-MP3	**ABTS**	6.5	1.57×10^6	34
E^2L-(*TD*)-Fe^{3+}–Mimochrome VI	**ABTS**	6.5	1.6×10^7	80
HRP	**guaiacol**	6.5	5.00×10^5	79
Fe^{3+}–Mimochrome VI	**guaiacol**	6.5	8.70×10^5	79
Xln10A-Fe(T*p*CPP)	**guaiacol**	7.5	2.4×10^3	109
rMB-H^{64}D	**guaiacol**	6.0	8.5×10^4	95
HRP	***o*-dianisidine**	N/A	1.6×10^4	109
Xln10A-Fe(T*p*CPP)	***o*-dianisidine**	7.5	2.2×10^4	109
MP8	***o*-dianisidine**	7.4	1.45×10^6	103
HRP	**pyrogallol**	N/A	2.20×10^6	140
PCN-222(Fe)	**pyrogallol**	N/A	4.85×10^4	140
Hemin	**pyrogallol**	7.4	N/A	140
HRP	**3,3,5,5-Tetra-methyl-benzidine**	3.5	5.58×10^8	140
PCN-222(Fe)	**3,3,5,5-Tetra-methyl-benzidine**	3	8.59×10^3	140
Hemin	**3,3,5,5-Tetra-methyl-benzidine**	N/A	1.26×10^2	140
HRP	***o*-phenylene-diamine**	N/A	2.37×10^8	140
PCN-222(Fe)	***o*-phenylene-diamine**	N/A	8.18×10^2	140

N/A= not available

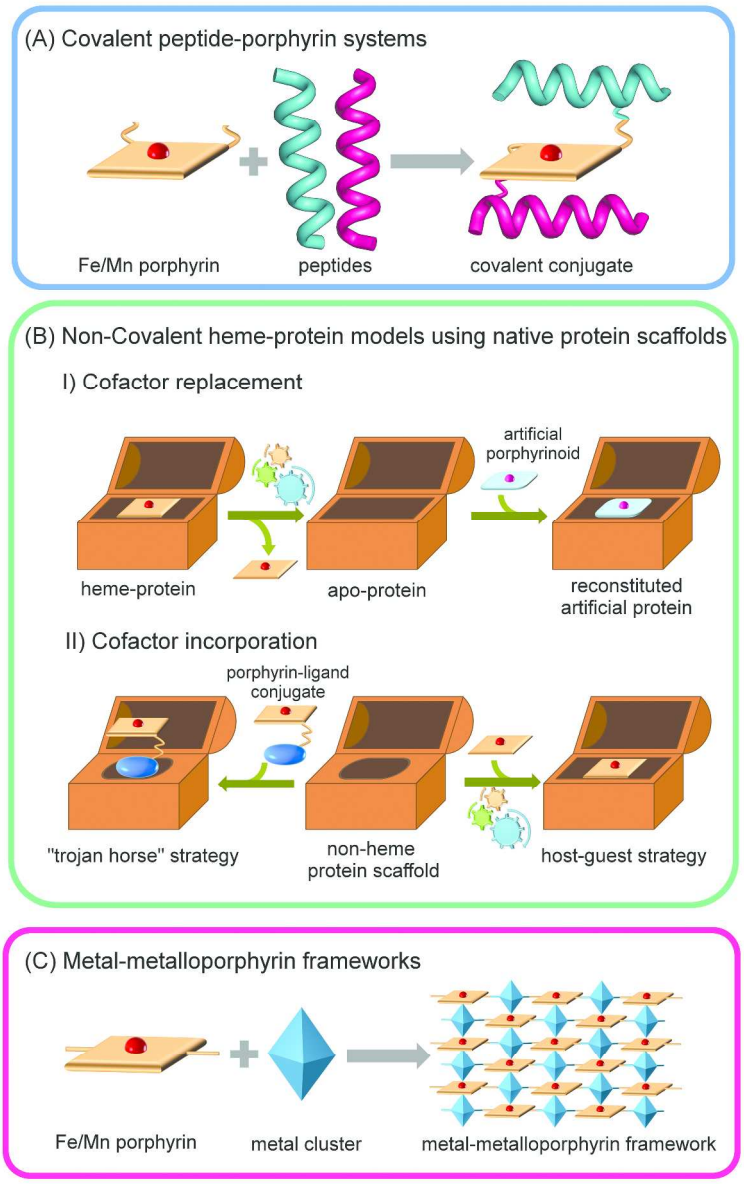

Figure 1. Designed or engineered enzyme-like cages classification. Schematic representation of (A) Covalent systems: short peptides or protein are covalently bound to the metal cofactor; (B) Non-covalent systems: the protein scaffold, represented as a chest, can be opportunely functionalized/"filled" with porphyrinoid rings by *i)* cofactor replacement, or *ii)* cofactor incorporation; (C) Metal-metalloporphyrin frameworks: a metal cluster node, represented as a blue prism, interconnects several metalloporphyrins, generating two- or three-dimensional lattices.

265x417mm (300 x 300 DPI)

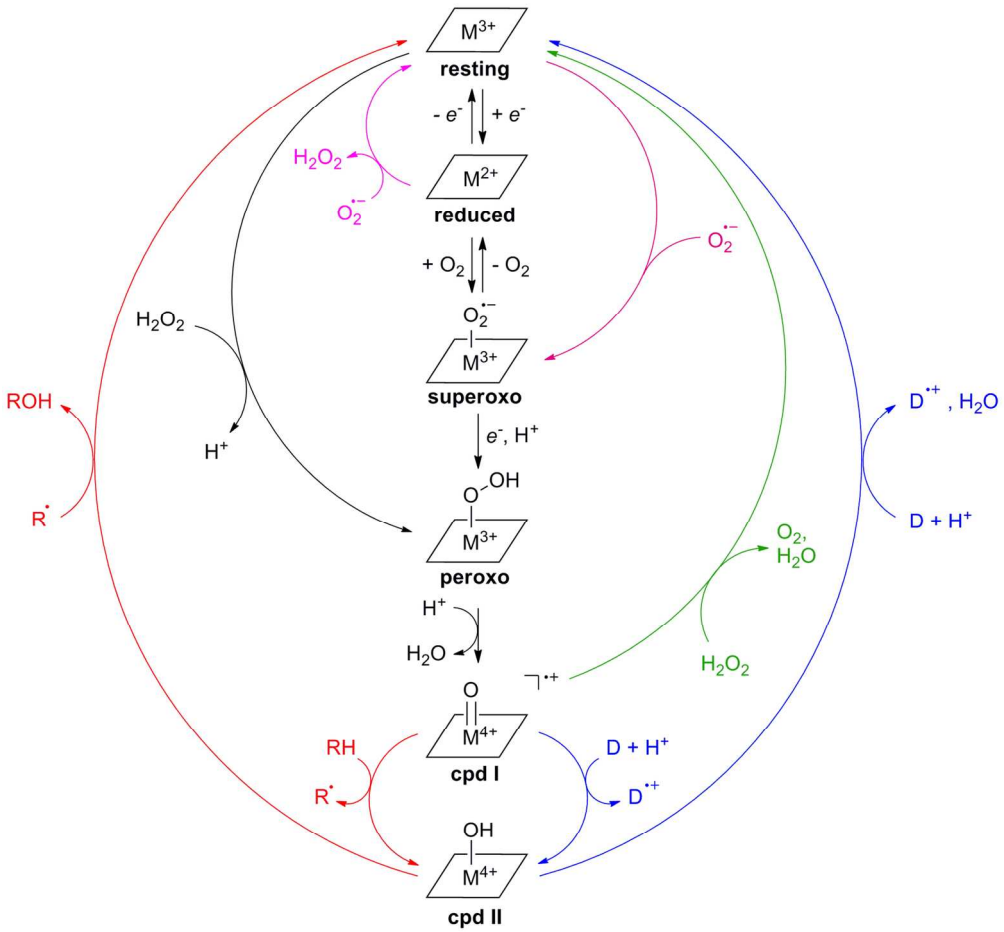

Figure 2. Heme paradigm for oxidation. Schematic representation of the different intermediates generated during the four different reaction pathways: superoxide dismutation (pink), peroxide dismutation (green), oxidase/peroxidase (blue), oxygenase/peroxygenase (red). Peroxide shunt, which allows bypassing the two reductive steps needed to activate dioxygen, is depicted as a black arrow.

156x145mm (300 x 300 DPI)

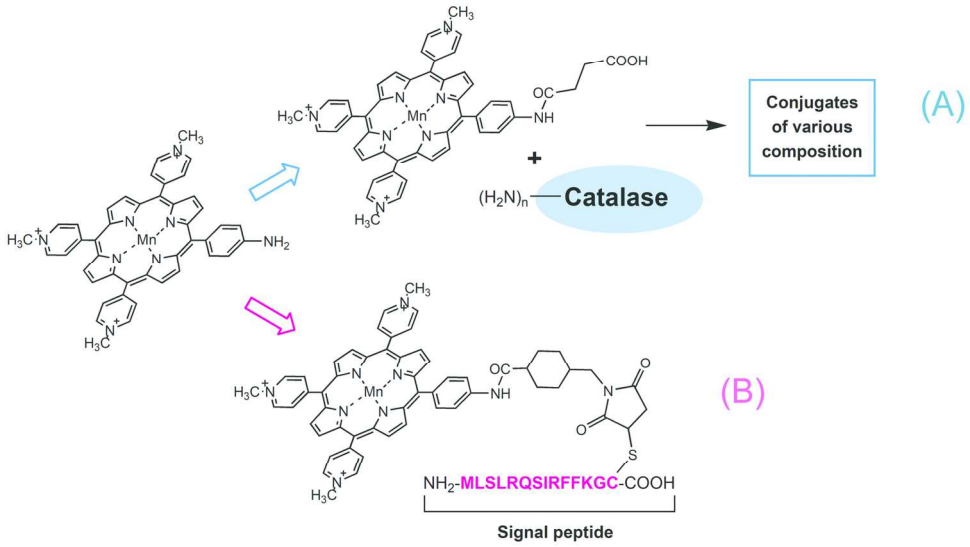

Figure 3. (A) Mn-porphyrin–catalase conjugate with the dual function of SOD and catalase; (B) Mn-porphyrin-oligopeptide conjugate with SOD activity.

150x90mm (300 x 300 DPI)

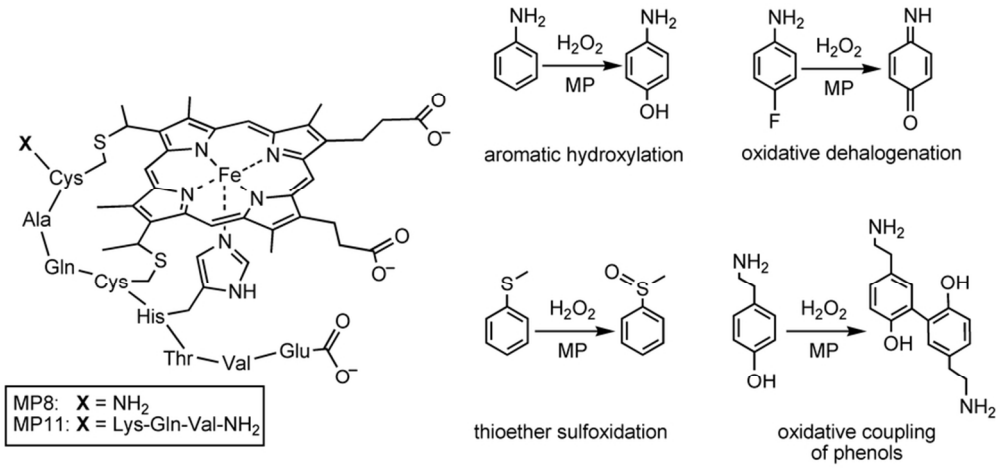

Figure 4. Microperoxidases and their catalyzed oxidation reactions.

82x38mm (300 x 300 DPI)

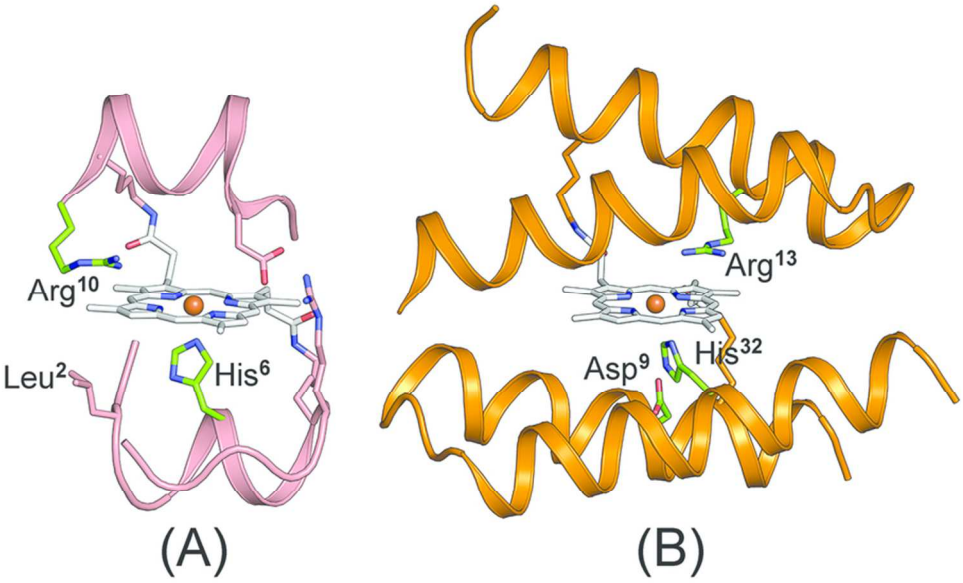

Figure 5. Miniaturized heme-proteins. Molecular models of: (A) E2L(TD)-Fe(III)-mimochrome VI with key residues depicted as sticks: the coordinating His6, the hydrophobic Leu2 at N-terminal position and the catalytic Arg10 on the distal site; (B) Fe(III)-MP3 with key residues of the first and second coordination spheres depicted as sticks: the His32 and the hydrogen-bonded Asp9 on the proximal site, the catalytic Arg13 on the distal site. The structures were generated using PyMol.[144]

80x47mm (300 x 300 DPI)

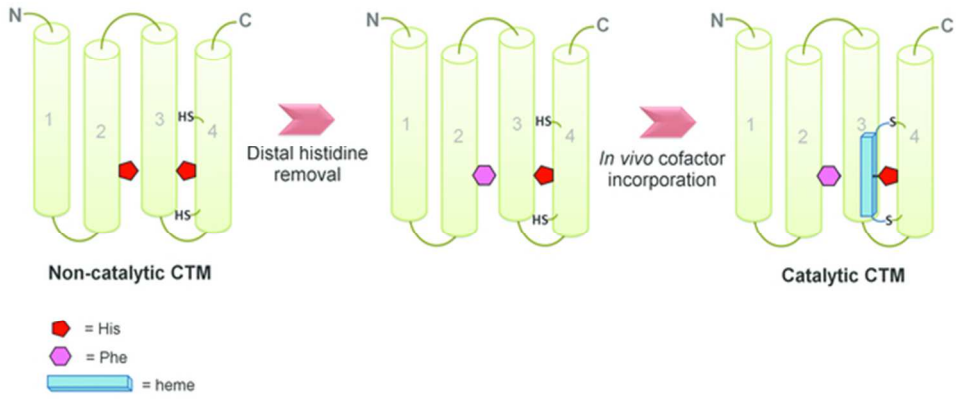

Figure 6. Design strategy for C-type cytochrome maquettes (CTMs). Adapted from ref. 34.

56x24mm (300 x 300 DPI)

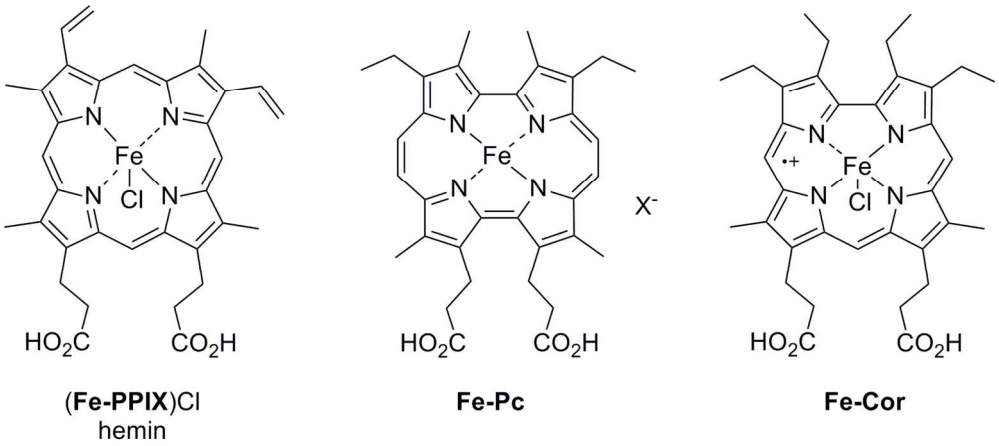

Figure 7. Native Fe(III)-protoporphyrin IX (Fe-PPIX) and the synthetic Fe(III)-porphycene (Fe-Pc) and Fe(III)-corrole (Fe-Cor).

139x62mm (300 x 300 DPI)

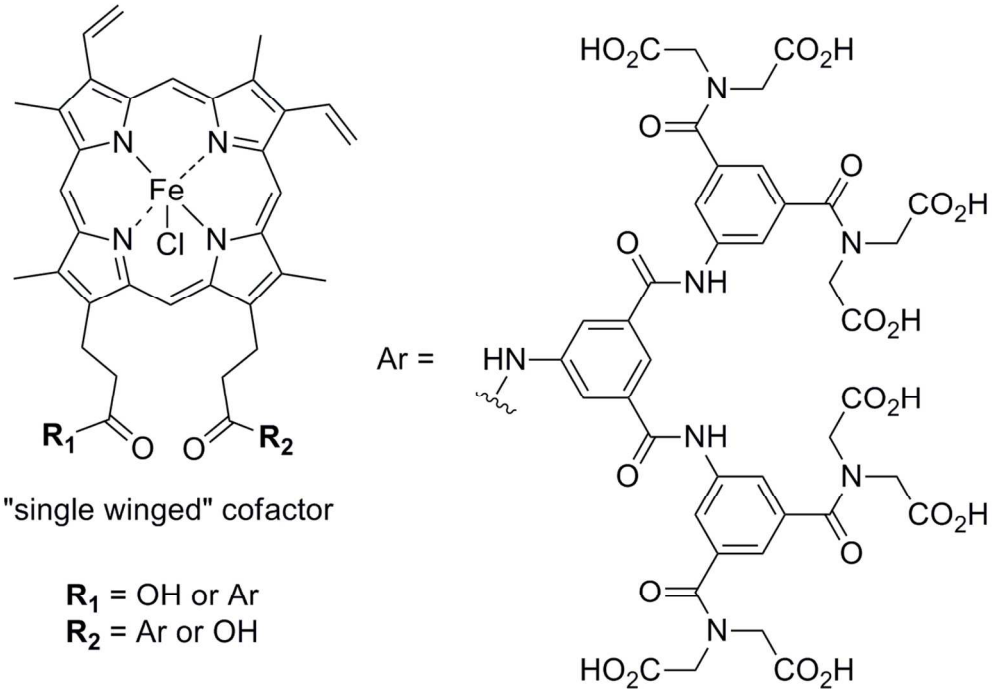

Figure 8. "Single winged" synthetic cofactor used in reconstitution of MbH64D.

113x78mm (300 x 300 DPI)

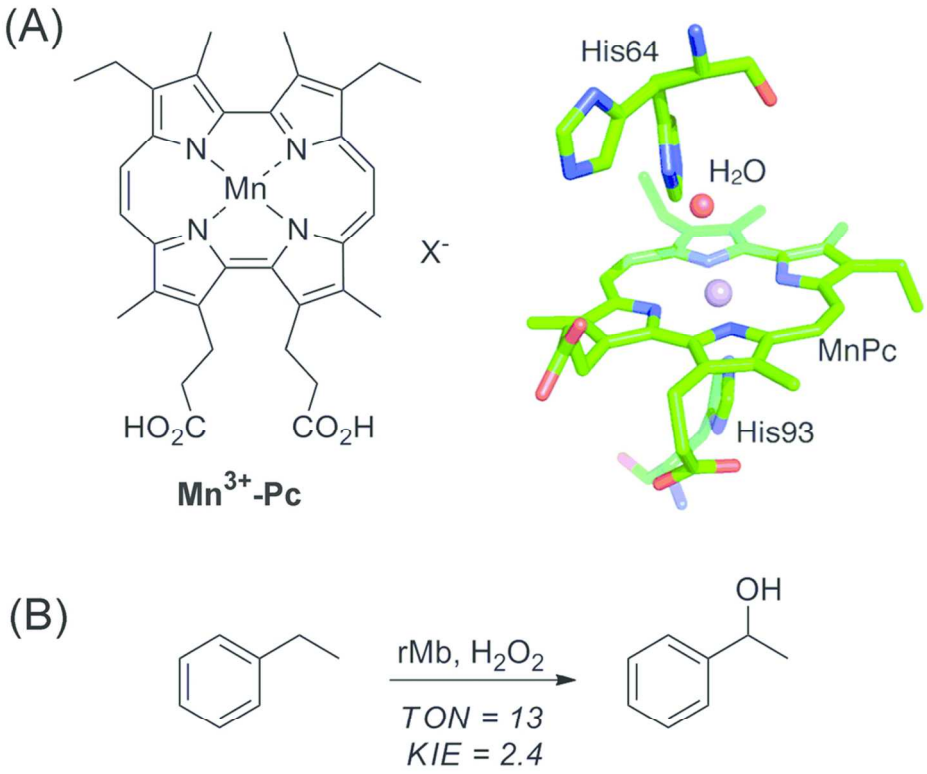

Figure 9. (A) Mn(III)-Pc cofactor used in reconstitution of Mb; (B) Hydroxylation of ethylbenzene catalyzed by Mn(III)-Pc-Mb. Adapted with permission from ref. 96. Copyright 2013 American Chemical Society.

94x82mm (300 x 300 DPI)

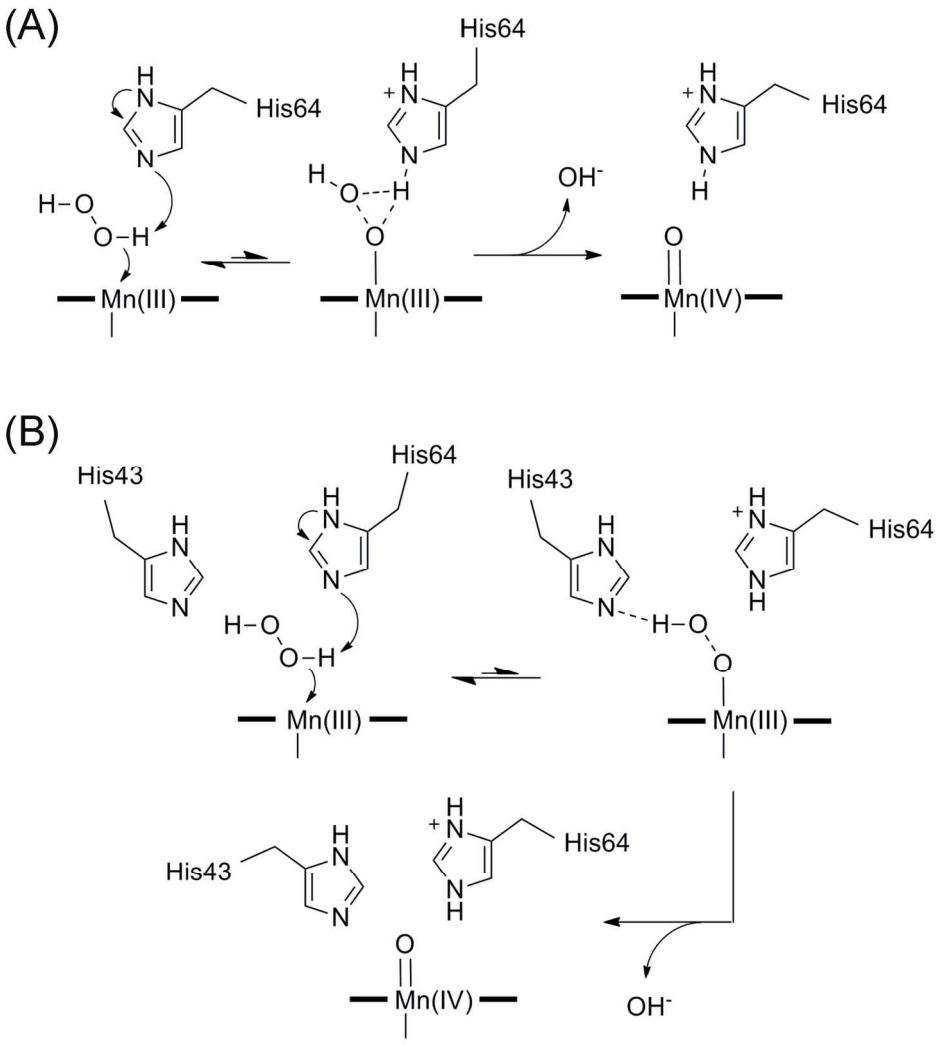

Figure 10. Mechanism of Mn(IV)=O intermediate formation in (A) Mn(III)-wtMb, assisted by distal histidine at the position 64, and in (B) Mn(III)-F43H-Mb mutant, assisted by two distal histidines at positions 64 and 43. Adapted with permission from ref. 97. Copyright 2013 RSC.

150x166mm (300 x 300 DPI)

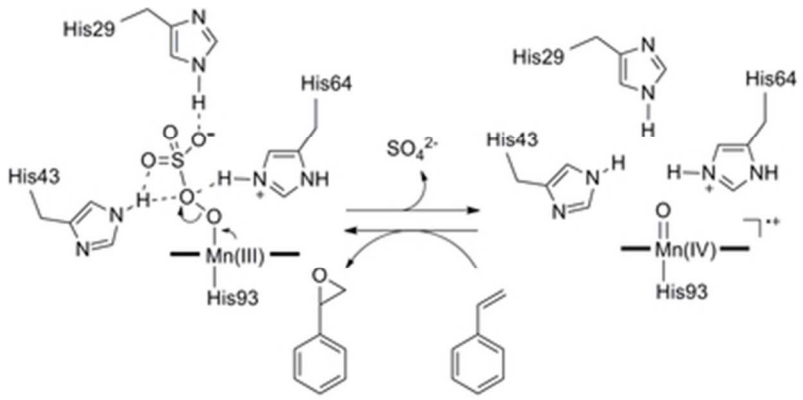

Figure 11. Oxone-mediated styrene epoxidation, through synergic assistance of His64, His29 and His43 residues, in the Mn(III)-L29H/F43H-Mb mutant. Adapted with permission from ref. 100. Copyright 2016 RSC.

33x16mm (300 x 300 DPI)

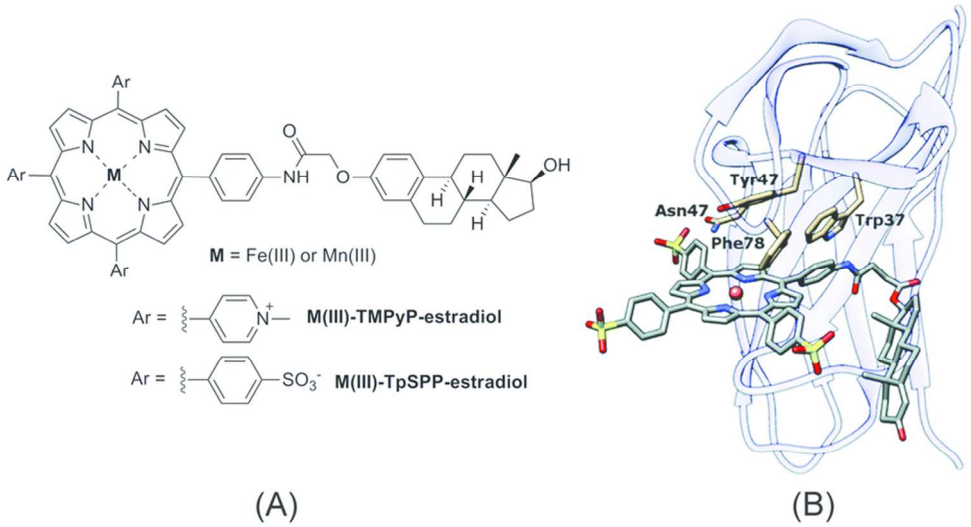

Figure 12. (A) Structure of metalloporphyrin-estradiol conjugates. (B) Docking model of Fe(III)-TpSPP-testosterone complexed with neocarzinostatin variant, NCS-3.24. Adapted with permission from ref. 6. Copyright 2015 RSC.

83x45mm (300 x 300 DPI)

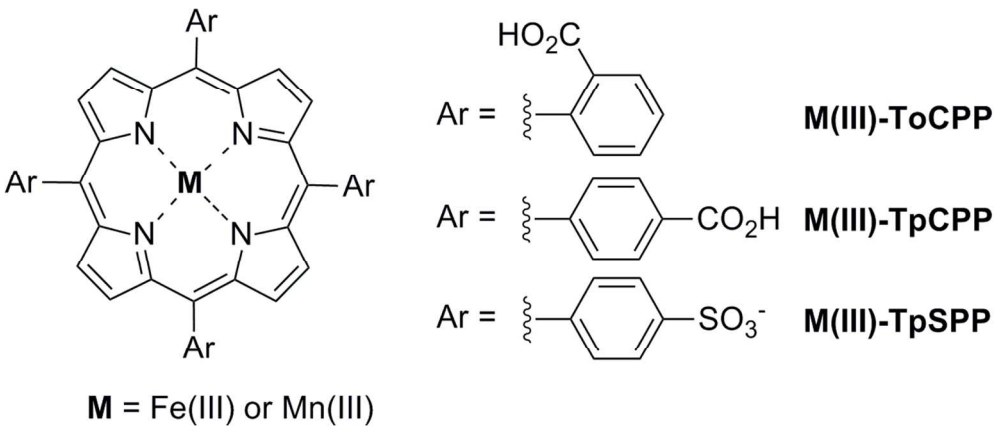

Figure 13. Fe(III)- and Mn(III)-porphyrins used in complex with Xln10A.

109x47mm (300 x 300 DPI)

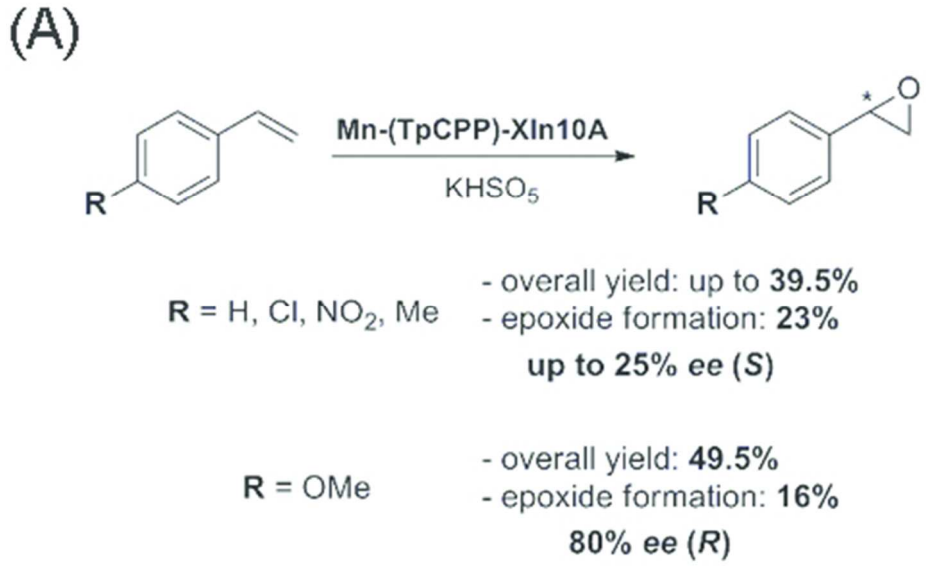

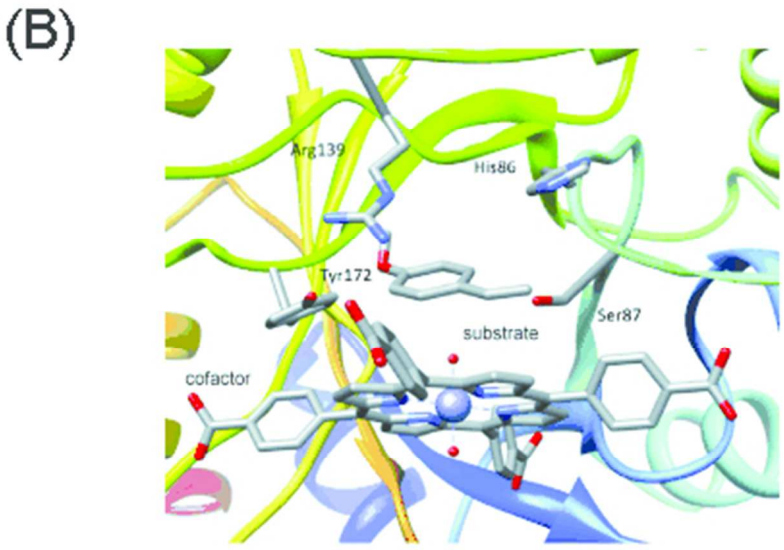

Figure 14. (A) Reaction scheme of styrene oxidation catalyzed by Mn-(TpCPP)-Xln10A enzyme, with the total yields in the oxidation products; (B) Docking model of p-methoxystyrene in the metallo-enzyme. Styrene orientation is consistent with R-epoxide formation. Adapted with permission from ref. 110. Copyright Wiley 2012.

85x105mm (150 x 150 DPI)

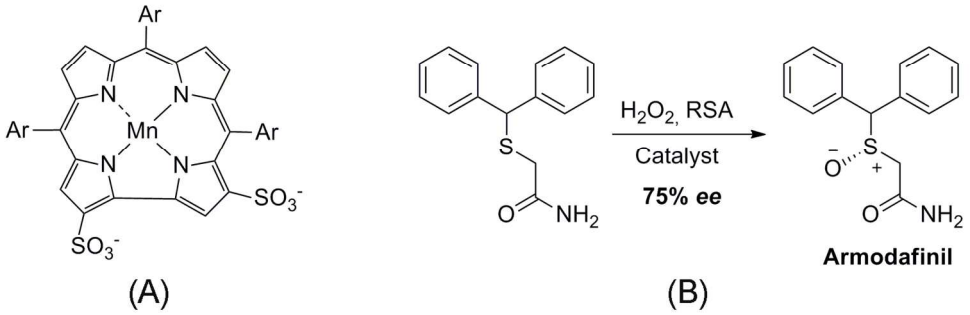

Figure 15. (A) Structure of Mn(III)-corrole catalyst for sulfoxidation reaction; (B) Reaction scheme of the asymmetric synthesis of Armodafinil.

151x51mm (300 x 300 DPI)

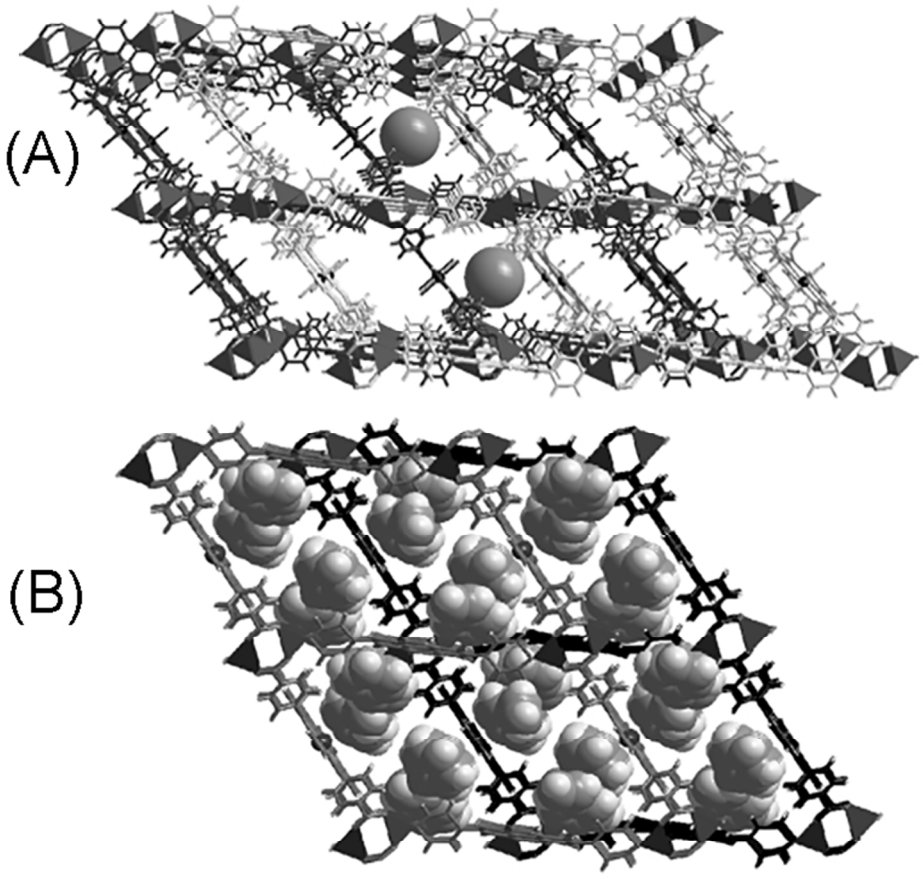

Figure 16. Crystal structures of (A) CZJ-1 (CCDC: 923792) and (B) styrene-included CZJ-1 (CCDC: 882227) viewed along the channels. Adapted with permission from ref. 136. Copyright 2013 Wiley.

70x71mm (300 x 300 DPI)

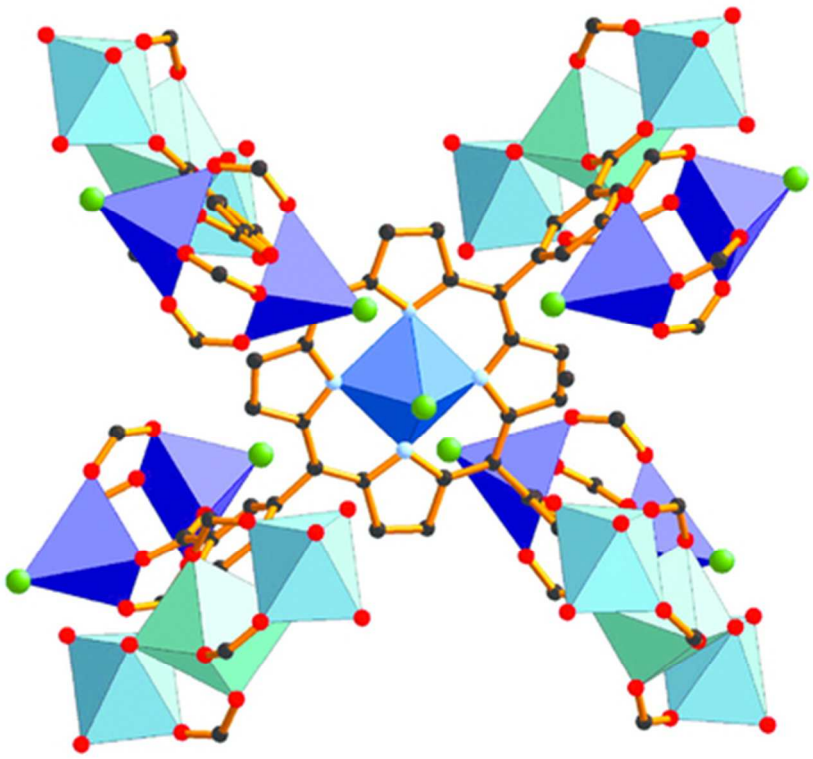

Figure 17. Crystal structure of ZJU-18 (CCDC: 898632). Mn(III)-meso-tetrakis-(3,5-dicarboxylphenyl)porphyrin connected to binuclear Mn2(COO)4 and trinuclear Mn3(COO)4(μ-H2O)2 units. The Mn-centered polyhedra are shown in different shades of blue. Reprinted with permission from ref. 139. Copyright 2012 American Chemical Society.

36x33mm (300 x 300 DPI)

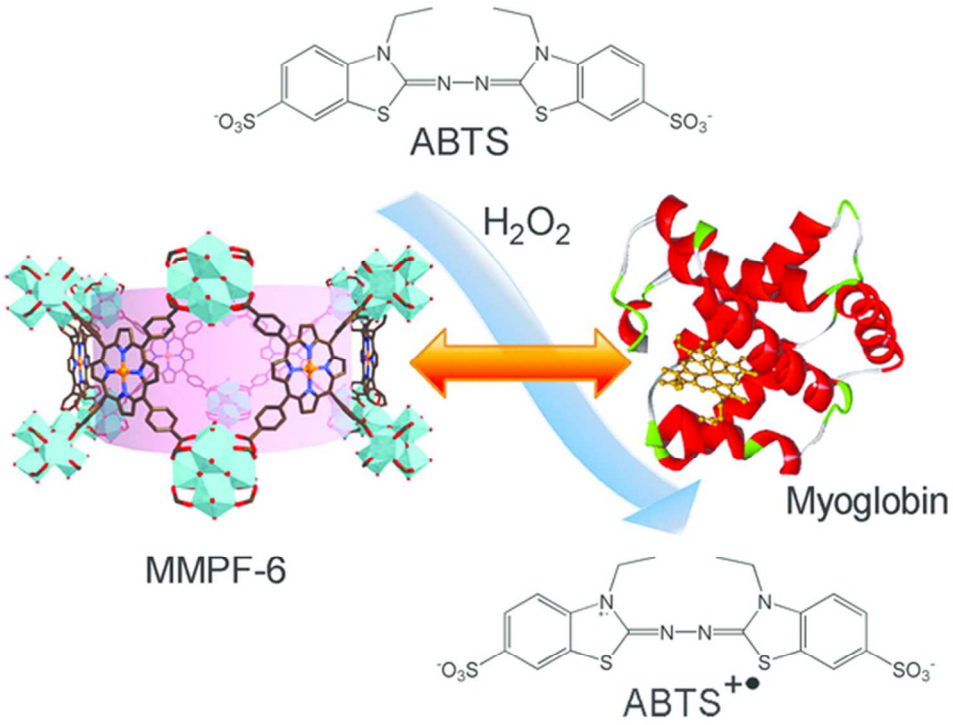

Figure 18. Biomimetic catalyst MMPF-6. Fe(III)-TpCPP-Cl connected with zirconium oxide clusters demonstrated peroxidase activity comparable to the natural myoglobin. Reprinted with permission from ref. 142. Copyright 2012 American Chemical Society.

55x43mm (300 x 300 DPI)